


# Aberrant association of misfolded SOD1 with Na<sup>+</sup>/K<sup>+</sup>ATPase- $\alpha$ 3 impairs its activity and contributes to motor neuron vulnerability in ALS

Céline Ruegsegger<sup>1,2</sup> · Niran Maharjan<sup>1,2</sup> · Anand Goswami<sup>3</sup> ·  
Audrey Filézac de L'Etang<sup>1,2,7</sup> · Joachim Weis<sup>3</sup> · Dirk Troost<sup>4</sup> · Manfred Heller<sup>5</sup> ·  
Heinz Gut<sup>6</sup> · Smita Saxena<sup>1</sup> 

Received: 23 August 2015 / Revised: 3 November 2015 / Accepted: 14 November 2015 / Published online: 30 November 2015  
© Springer-Verlag Berlin Heidelberg 2015

**Abstract** Amyotrophic lateral sclerosis (ALS) is an adult onset progressive motor neuron disease with no cure. Transgenic mice overexpressing familial ALS associated human mutant SOD1 are a commonly used model for examining disease mechanisms. Presently, it is well accepted that alterations in motor neuron excitability and spinal circuits are pathological hallmarks of ALS, but the underlying molecular mechanisms remain unresolved. Here, we sought to understand whether the expression of mutant SOD1 protein could contribute to altering processes governing motor neuron excitability. We used the conformation specific

antibody B8H10 which recognizes a misfolded state of SOD1 (misfSOD1) to longitudinally identify its interactome during early disease stage in SOD1G93A mice. This strategy identified a direct isozyme-specific association of misfSOD1 with Na<sup>+</sup>/K<sup>+</sup>ATPase- $\alpha$ 3 leading to the premature impairment of its ATPase activity. Pharmacological inhibition of Na<sup>+</sup>/K<sup>+</sup>ATPase- $\alpha$ 3 altered glutamate receptor 2 expression, modified cholinergic inputs and accelerated disease pathology. After mapping the site of direct association of misfSOD1 with Na<sup>+</sup>/K<sup>+</sup>ATPase- $\alpha$ 3 onto a 10 amino acid stretch that is unique to Na<sup>+</sup>/K<sup>+</sup>ATPase- $\alpha$ 3 but not found in the closely related Na<sup>+</sup>/K<sup>+</sup>ATPase- $\alpha$ 1 isozyme, we generated a misfSOD1 binding deficient, but fully functional Na<sup>+</sup>/K<sup>+</sup>ATPase- $\alpha$ 3 pump. Adeno associated virus (AAV)-mediated expression of this chimeric Na<sup>+</sup>/K<sup>+</sup>ATPase- $\alpha$ 3 restored Na<sup>+</sup>/K<sup>+</sup>ATPase- $\alpha$ 3 activity in the spinal cord, delayed pathological alterations and prolonged survival of SOD1G93A mice. Additionally, altered Na<sup>+</sup>/K<sup>+</sup>ATPase- $\alpha$ 3 expression was observed in the spinal cord of individuals with sporadic and familial ALS. A fraction of sporadic ALS cases also presented B8H10 positive misfSOD1 immunoreactivity, suggesting that similar mechanism might contribute to the pathology.

C. Ruegsegger and N. Maharjan contributed equally to this study.

**Electronic supplementary material** The online version of this article (doi:10.1007/s00401-015-1510-4) contains supplementary material, which is available to authorized users.

✉ Smita Saxena  
smita.saxena@izb.unibe.ch

- <sup>1</sup> Institute of Cell Biology, University of Bern, Bern, Switzerland
- <sup>2</sup> Graduate School for Cellular and Biomedical Sciences, University of Bern, Bern, Switzerland
- <sup>3</sup> Institute of Neuropathology, Rheinisch-Westfälische Technische Hochschule, Aachen University Hospital, Aachen, Germany
- <sup>4</sup> Division of Neuropathology, Department of Pathology, Academic Medical Center, Amsterdam, The Netherlands
- <sup>5</sup> Department of Clinical Research, Inselspital, University of Bern, Bern, Switzerland
- <sup>6</sup> Friedrich Miescher Institute for Biomedical Research, Basel, Switzerland
- <sup>7</sup> Present Address: Department of Neuroscience, Genentech, Inc., South San Francisco, California, USA

**Keywords** ALS · Na<sup>+</sup>/K<sup>+</sup>ATPase- $\alpha$ 3 · SOD1 interactome · Motor neuron excitability · Sporadic and familial ALS

## Introduction

Amyotrophic lateral sclerosis (ALS) is an adult onset progressive fatal motor neuron (MN) disease with an incidence of one to two persons per 100,000 [40] and is characterized by MN degeneration in the spinal cord, motor cortex and

the brain stem [69]. Death usually occurs within 3–5 years after diagnosis and no cure or treatment is available [43]. Transgenic mice overexpressing familial ALS (fALS) associated human mutant SOD1 (mutSOD1) under the control of a human SOD1 promoter serve as a valuable animal model for examining ALS disease mechanisms [27, 57]. These mice reproduce characteristic disease features, such as silent presymptomatic phases of increasing cell specific stress and dysfunction, and rapidly progressing clinical phases followed by paralysis and death. MutSOD1 exhibits a high propensity to undergo conformational changes leading to aggregation of the protein [51, 52]. Over 160 SOD1 point mutations have been identified and misfSOD1 aggregates have been found specifically in disease vulnerable neurons in patients and animal models of disease suggesting that conformational changes in SOD1 renders the enzyme cytotoxic via a gain of function mechanism [2, 22, 28]. Therapeutic approaches based on targeting the toxic protein species in mice via infusion of conformation specific antibodies against mutSOD1 [24, 38, 53, 63] or viral mediated knock down of mutSOD1 [54] have been successful in alleviating disease and extending life span.

The consistent temporal reproducibility of dysfunctions in MNs in SOD1G93A animals has enabled longitudinal studies, revealing that low-excitability or high-firing-threshold fast fatiguable (FF) MNs are most vulnerable to denervation. Medium excitable fatigue-resistant (FR) MNs and highly-excitability or low-firing-threshold slow (S) MNs resist denervation over a certain time period [50]. FF MNs denervate their target muscle fiber before any visible symptoms, followed by FR MNs precisely 30–35 days later and S MNs partially loose contact with target muscles at end stage [29, 50], suggesting that MN vulnerability in ALS is inversely proportional to MN excitability. Furthermore, MNs in ALS exhibit ER stress [3, 31] and specifically FF MNs are most prone to ER stress associated unfolded protein response (UPR) [19, 56]. However, the underlying mechanism behind the higher vulnerability of the low excitable FF MNs to degeneration in ALS have not been elucidated.

Presently, one focus in the field of ALS is to understand the precise interplay between MN electro-chemical properties, alterations in MN excitability and impairments in intracellular calcium signaling [21, 34, 35, 58]. MutSOD1 expressing MNs show alterations in MN excitability as from second postnatal week [8, 46] and similar early alterations in MN excitability have been observed in sporadic and familial ALS patients [13, 66, 67, 68]. Recently, it was shown that early hyperexcitability of MNs is neuroprotective and that reduced excitability aggravates ALS related pathology [58]. Furthermore, disease resistant S MNs exhibit an early intrinsic hyperexcitability in mutSOD1 neonates while disease vulnerable FF MNs are not hyperexcitable in neonate

mutSOD1 mice [35]. Focusing on vulnerable trigeminal MNs in mutSOD1 mice, it was found that firing threshold decreased selectively within high-threshold trigeminal MNs, while it increased in a subpopulation of low-threshold trigeminal MNs at early presymptomatic stages. However, those alterations were not observed in disease resistant oculomotor neurons [65], suggesting that alterations in MN excitability are early indications of disease associated responses within affected MNs in ALS. Further, it has been shown that the accumulation of misfSOD1 as detected by conformation specific antibodies closely parallels excitability signaling deficits in vulnerable fALS MNs [47, 58], indicating that the expression of mutSOD1 might also interfere at some level with molecular components involved in neuronal excitability [39, 45, 64]. A recent study employing binary epitope mapping technique identified several conformation specific pathogenic species of SOD1 whose presence directly correlated with disease progression and life span of mutant mice [5]. Further, emerging evidences suggest that non-genetic dysfunctions such as metal depletion, oxidation and disruption of the quaternary structure cause wild-type SOD1 protein to misfold and to adopt a toxic conformation as observed in mutSOD1 related fALS, indicating that SOD1 might be a shared pathogenic factor between the two forms of ALS; sporadic and familial [18, 25, 55].

Despite a growing number of studies describing alterations in MN excitability, the relevant relationship between the presence of misfSOD1 and alterations in MN excitability and the identity of molecular players associated with these alterations in disease remains unknown. Here, we used a proteomic approach to explore the link between the presence of misfSOD1 and alterations in MN excitability. Using the misfSOD1 conformation specific antibody B8H10 [24], we mapped the unique interactome of misfSOD1 (G93A variant) longitudinally in mutant mice, thereby identifying a conserved signature of the misfSOD1 interactome. From the earliest time point (P15), when a distinct B8H10 positive misfSOD1 signal is detected in a subpopulation of mutant MNs, misfSOD1 formed a complex with Na<sup>+</sup>/K<sup>+</sup>ATPase- $\alpha$ 3. The direct association of misfSOD1 to Na<sup>+</sup>/K<sup>+</sup>ATPase- $\alpha$ 3 led to an early and progressive impairment in Na<sup>+</sup>/K<sup>+</sup>ATPase- $\alpha$ 3 activity. Pharmacological inhibition of Na<sup>+</sup>/K<sup>+</sup>ATPase- $\alpha$ 3 worsened disease pathology and altered molecular components involved in neuronal transmission. By mapping the site of association of misfSOD1 with Na<sup>+</sup>/K<sup>+</sup>ATPase- $\alpha$ 3 onto a 10 amino acid stretch that is unique to Na<sup>+</sup>/K<sup>+</sup>ATPase- $\alpha$ 3 but not found in the closely related Na<sup>+</sup>/K<sup>+</sup>ATPase- $\alpha$ 1 isozyme, we generated a functional misfSOD1 binding deficient Na<sup>+</sup>/K<sup>+</sup>ATPase- $\alpha$ 3 protein. Viral mediated expression of the chimeric pump in two different SOD1G93A models restored Na<sup>+</sup>/K<sup>+</sup>ATPase- $\alpha$ 3 activity, delayed disease manifestations and increased life span. Moreover, altered Na<sup>+</sup>/K<sup>+</sup>ATPase- $\alpha$ 3 levels and misfSOD1

positive immunoreactivity were observed in the spinal cord of individuals with sporadic ALS (sALS) and non-SOD1 mediated fALS cases.

## Materials and methods

### Mice strains

The moderate expresser transgenic mice line of human SOD1 carrying a Gly93-Ala mutation (*B6SJL-Tg(SOD1-G93A)<sup>dl1</sup>Gur/J*), the high expresser transgenic mice line of human SOD1 (*B6SJL-Tg(SOD1\*G93A)1Gur/J*) crossed into *C57BL/6J* background and *B6.Cg-Tg(SOD1\*G37R)1Dwc/J* were from Jackson Laboratory. The average life spans of *SOD1* transgenic mice in our colony were 270–280 days for medium expresser mice (8–10 copies), 145–152 days for high expresser mice (20 copies). Animal care, housing (IVC cages, 5 mice/cage), 12 h light/12 h dark cycle, ethical usage and procedures were approved and performed in accordance to the Swiss Veterinary Law guidelines.

### Human samples and immunofluorescent staining

Human post mortem samples ( $n = 9$  lumbar spinal cords for sporadic (sALS), 4 for controls, 6 for *C9ORF72* and 2 for *FUS* mutations) were obtained from the Amsterdam Academic Medical Center (AMC), Institute of Neuropathology, Division of Neuropathology, Department of Pathology ALS Bank following the guidelines of the local ethics committee. The spinal cords of these clinically confirmed sALS patients, as well as age-matched controls had been obtained within 6–12 h after death. Tissues were used in compliance with the Declaration of Helsinki. All ALS patients suffered from clinical signs and symptoms of lower and upper MN disease with the eventual involvement of brain stem motor nuclei. Importantly, none of these patients had cognitive impairment or dementia. Age-matched control patients did not show any neuropathological anomalies. Transverse paraffin sections (3–4  $\mu\text{m}$  in thickness) of human (lumbar) spinal cord were cut on a microtome. Sections were placed on silane-coated slides, de-waxed, rehydrated and heated in citrate buffer for antigen retrieval. Processed sections were incubated with primary antibodies for 1 h at room temperature. Appropriate HRP secondary antibodies were used (1:200, Vector Laboratories, USA) for 1 h, followed by DAB visualization (DAKO, Denmark). For immunofluorescence secondary antibodies conjugated with Alexa fluorophore (Invitrogen) were used. Staining patterns were visualized using a Zeiss LSM 700 confocal microscope. The resulting confocal images were processed using the Zeiss LSM software and Adobe Photoshop CS5. DAB immunohistochemical

sections were photographed using an Axioplan microscope (Zeiss) with an Axio Cam HR camera using 63 $\times$  oil immersion lens (Zeiss).

### Reagents and pharmacological treatments

Drug administration protocols in all mice were as follows: Salubrial (Alexis Biochemicals, dissolved at 10 mg/ml in DMSO), injected intraperitoneally (i.p.) in saline at 1 mg/kg. Ouabain (Tocris Bioscience; dissolved in ethanol at 20 mg/ml), injected i.p. or intraspinal in PBS at 0.5 mg/kg or 0.01–0.05 mg/kg. Tunicamycin (Ascent scientific) injected i.p. in saline at 1 mg/kg. RITC Dextran or Cholera Toxin Subunit B (Invitrogen) was injected locally into lateral gastrocnemius or soleus, as previously described [56].

### Na<sup>+</sup>/K<sup>+</sup>ATPase activity measurement

The Na<sup>+</sup>/K<sup>+</sup>ATPase activity was determined by colorimetric assay [20]. 50  $\mu\text{g}$  of synaptosomes were suspended in 350  $\mu\text{l}$  of 30 mM Tris-HCl, 0.1 mM EDTA, 50 mM NaCl, 5 mM KCl, 6 mM MgCl<sub>2</sub> in the presence or absence of 1 or 3 mM Ouabain (Na<sup>+</sup>/K<sup>+</sup>ATPase inhibitor) that has a dose-dependent and isoform-specific action. Na<sup>+</sup>/K<sup>+</sup>ATPase- $\alpha$ 3 has the highest sensitivity to low concentrations of Ouabain (IC<sub>50</sub> values: 0.1–1  $\mu\text{M}$  for  $\alpha$ 3 and 32  $\mu\text{M}$  for  $\alpha$ 1) [37, 62]. After sonication, the reaction was initiated by 3 mM ATP and incubated 40 min at 37 °C. The reaction was stopped with 50  $\mu\text{l}$  of 50 % TCA, and samples centrifuged at 1000g for 10 min at 4 °C. 90  $\mu\text{l}$  of supernatant was mixed with 200  $\mu\text{l}$  of coloring solution (mix 20 ml of ascorbic acid pH 5 with 5 ml of 35 mM ammonium molybdate/15 mM zinc acetate). Absorbance was read at 700 nm via a SpectraMax Microplate reader (Molecular Devices). NaH<sub>2</sub>PO<sub>4</sub> was the reference standard and blank was a reaction without ATP. Specific Na<sup>+</sup>/K<sup>+</sup>ATPase- $\alpha$ 3 activity was obtained by subtracting the 1 mM Ouabain sensitive activity from the global Na<sup>+</sup>/K<sup>+</sup>ATPase activity and was expressed in nmol of Pi/min/mg of protein.

### Immunoprecipitation and western blotting

IP and western blotting was performed from ventral horn of spinal cords as described [24]. Primary antibodies used for western blot; mouse anti-B8H10, 1:500 (Mediabios), rabbit anti-SOD1, 1:1500 (Enzo Life Sciences), rabbit anti-SOD1 (HPA001401), 1:2000 (Sigma), rabbit anti-Na<sup>+</sup>/K<sup>+</sup>ATPase- $\alpha$ 3 (ab78798), 1:2000 (Abcam), goat anti-Na<sup>+</sup>/K<sup>+</sup>ATPase- $\alpha$ 3 (sc-16052), 1:500 (Santa Cruz), rabbit anti-Actin, 1:10,000 (Sigma), rabbit anti-Myc (clone A-14), 1:1000 (Santa Cruz), mouse anti-Myc tag (9B11), 1:5000 (Cell Signaling), mouse anti-Na<sup>+</sup>/K<sup>+</sup>ATPase- $\alpha$ 1, 1:500 (Santa Cruz), rabbit anti-GFP, 1:5000 (Cell Signaling), mouse anti-Tubulin, 1:10,000 (Sigma). For input, 5 % of total protein extracts was loaded on the SDS-PAGE gel.

## Mass spectrometry analysis

Whole co-IP were loaded on 12 % SDS gel and run for 1 cm. Gel was prefixed using fixer for 2 h, washed with miliQ H<sub>2</sub>O for 1 h. Lanes were cut into 9 pieces and each piece was again cut into 4 pieces. Gels were washed with 100 % ethanol for 30 min followed by washing with miliQ H<sub>2</sub>O for 30 min (cycle repeated 3 times). Gel slices were kept in 20 % ethanol for further MS analyses. The proteins in each gel slice were digested by trypsin, extracted and analyzed by nanoLC-MS/MS on a LTQ-orbitrap XL system as described [26]. For the individual gel bands, peptides were separated by a short 10 min 5 to 40 % acetonitrile gradient, while the samples from the entire gel proteome analyses were separated by a 40 min gradient. Peak list files in the mgf format were produced either as described in [1] or by ProteomeDiscoverer 1.4 (ThermoFisher Scientific) and searched against the protein sequences of the reference proteome of mus musculus exported as fasta file from UniprotKB release (2011\_02) complemented with common contaminating proteins, like human keratins and pig trypsin. Database searching was performed with Phenix/Easyprot software (University of Geneva) as described in [1] using acetylation of the protein N-terminus, carbamidomethylation of Cys, de-amidation on Asn/Gln, oxidation of Met, phosphorylation of Ser/Thr/Tyr, and pyro-glutamic acid on Asp/Glu as variable modifications in the second search round. Protein identifications with at least two unique peptides at a FDR of 1 % (on peptide level) were extracted into MIAPE conform Excel files.

## Plasmid constructs

Mouse Na<sup>+</sup>/K<sup>+</sup>ATPase- $\alpha$ 3 cDNA clone was obtained from Source BioScience. Expression plasmid encoding the N-domain of Na<sup>+</sup>/K<sup>+</sup>ATPase- $\alpha$ 3 (Na<sup>+</sup>/K<sup>+</sup>-N residues 372–586) was obtained by PCR amplification introducing AsiSI and MluI restriction sites at the 5' and 3' ends. This fragment was then inserted into pCMV6-entry plasmid (Origene, RC204204) in front of the myc-tag. Na<sup>+</sup>/K<sup>+</sup>- $\Delta$ N-myc lacking residues 375–583 were synthesized and sub-cloned in pcDNA3.1<sup>+</sup>. Na<sup>+</sup>/K<sup>+</sup>ATPase- $\alpha$ 3-swap loop, consisting of the Na<sup>+</sup>/K<sup>+</sup>ATPase- $\alpha$ 3 with amino acids 484–493 exchanged with the amino acids 494–503 from mouse Na<sup>+</sup>/K<sup>+</sup>ATPase- $\alpha$ 1 was generated and cloned into pcDNA3.1<sup>+</sup> by GeneArt<sup>®</sup> Gene Synthesis (Life technologies).

## Isolation of synaptosomes and immunoprecipitation of synaptosomal fractions

Synaptosomes were isolated from ventral and dorsal horn of fresh spinal cords using the Syn-PER Reagent (Thermo Scientific). Synaptosomes were kept at 0–4 °C throughout

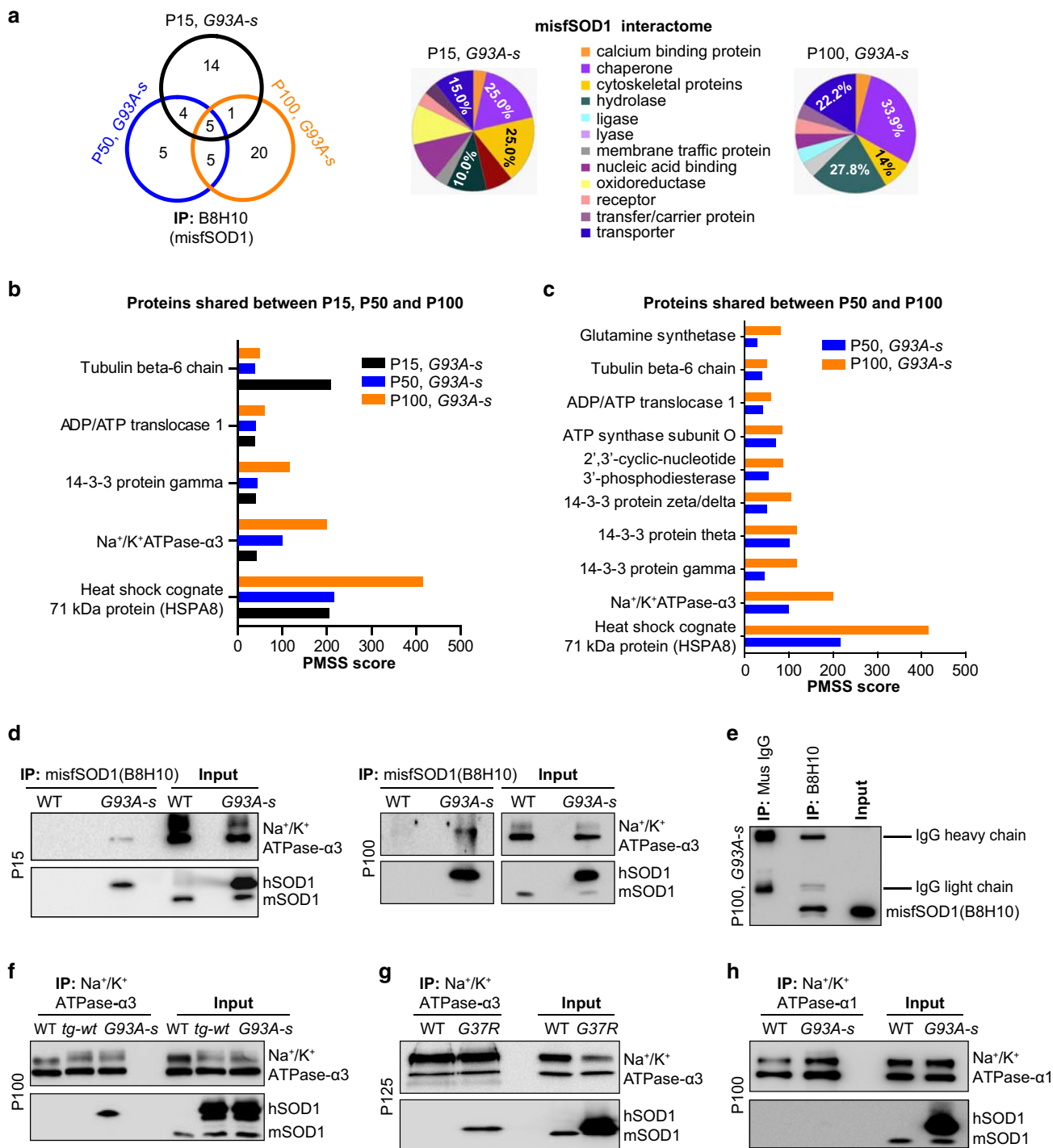
**Fig. 1** Identification of early aberrant interactions of misfSOD1. **a** Venn diagram of proteins interacting with misfSOD1 at P15, P50 and P100 identified by mass spectrometry (MS) after co-IP with B8H10 antibody from WT and *G93A-s* spinal cord. *Right* misfSOD1 interacting proteins grouped according to protein classes after PANTHER analysis. **b** Five shared and conserved interactions of misfSOD1 at all three ages, plotted by PMSS score. Each experiment done from ventral horn lysates of 4 mice/age and analyzed by MS in parallel. Each experiment repeated twice, values plotted for a single experiment. **c** Ten conserved interactions of misfSOD1 between P50 and P100 plotted by PMSS score. **d** Co-IP of misfSOD1 with B8H10 antibody from WT and *G93A-s* ventral horn at P15 (earliest detection of the B8H10 immunopositive misfSOD1) and P100, IB for Na<sup>+</sup>/K<sup>+</sup>ATPase- $\alpha$ 3 and SOD1, detecting both human SOD1 (hSOD1) and endogenous mouse SOD1 (mSOD1). Note the increase in misfSOD1-Na<sup>+</sup>/K<sup>+</sup>ATPase- $\alpha$ 3 complex at P100 compared to P15 in *G93A-s* lysates. **e** Co-IP using mouse IgG on P100 *G93A-s* spinal lysates. Parallel IP done with B8H10 antibody from same spinal lysates. IB with B8H10 reveals no unspecific association of misfSOD1 with mouse IgG. **f** Co-IP with Na<sup>+</sup>/K<sup>+</sup>ATPase- $\alpha$ 3 from WT, *tg-wt* and *G93A-s* spinal cord, IB for Na<sup>+</sup>/K<sup>+</sup>ATPase- $\alpha$ 3 and SOD1. Note no association of Na<sup>+</sup>/K<sup>+</sup>ATPase- $\alpha$ 3 with normal hSOD1 in *tg-wt* condition. **g** Presence of a misfSOD1-Na<sup>+</sup>/K<sup>+</sup>ATPase- $\alpha$ 3 complex in another SOD1 mutant model; *G37R*. **h** Co-IP with Na<sup>+</sup>/K<sup>+</sup>ATPase- $\alpha$ 1 from WT and *G93A-s* spinal lysates, IB with SOD1 reveals no interaction of Na<sup>+</sup>/K<sup>+</sup>ATPase- $\alpha$ 1 with misfSOD1 at P100. Representative blot from 4 experiments (**d**) or 3 experiments (**e–h**)

the procedure and used for all assays. Antibodies used for characterization of synaptosomes were mouse anti-Lamin A/C, 1:1500 (Santa Cruz), rabbit anti-Synaptophysin, 1:5000 (Dako), rabbit anti-VACHT, 1:2000 (Sigma), goat anti-Na<sup>+</sup>/K<sup>+</sup>ATPase- $\alpha$ 3 (sc-16052), 1:500 (Santa Cruz), mouse anti-GFAP, 1:1000 (Santa Cruz) and rabbit anti-SOD1, 1:2000 (Sigma), rabbit anti-VACHT, 1:2000 (Sigma), goat anti-Na<sup>+</sup>/K<sup>+</sup>ATPase- $\alpha$ 3 (sc-16052), 1:500 (Santa Cruz). Synaptosomes were incubated with 1 % Triton X-100 for 20 min on ice and centrifuged at 14,000g for 15 min to obtain the supernatant. 60  $\mu$ l of paramagnetic beads coated with G protein (Dynabeads; Invitrogen) were added to 200  $\mu$ g of sample, and the mixture was precleared at 4 °C for 2 h. The mixture was centrifuged at 15,300g for 30 s and the supernatant was mixed with appropriate antibody and incubated at 4 °C overnight. 60  $\mu$ l of anti-mouse or anti-rabbit IgG beads was added and incubated for 2 h, centrifuged at 15,300g for 30 s. The beads were recovered by centrifugation, washed thrice in PBS-1 % Triton X-100 buffer, resuspended in 2 $\times$  Laemmli buffer, separated on 12 % SDS-PAGE gels and analyzed by IB.

## Surface biotinylation of spinal cord slices

Mice were sacrificed and spinal cords were immediately placed into ice-cold Krebs's solution containing (mM): 125 NaCl, 4 KCl, 1.25 KH<sub>2</sub>PO<sub>4</sub>, 1.5 MgSO<sub>4</sub>, 26 NaHCO<sub>3</sub>, 1.5 CaCl<sub>2</sub> and 10 glucose. 500  $\mu$ m spinal cord slices were cut using McIlwain chopper. Slices were equilibrated in Krebs's solution bubbled with 95 % oxygen and 5 % carbon





dioxide in a 30 °C water bath before biotinylation in 1 mg/ml biotin solution (Pierce) at 4 °C. Spinal cord ventral horns were microdissected and homogenized as above, and equal amounts of protein were incubated with NeutrAvidin-agarose beads (Pierce) to immunoprecipitate biotinylated proteins. IP were separated on 10–12 % SDS-PAGE gels and analyzed by immunoblotting (IB) using the appropriate antibodies.

### Cloning, protein expression, purification and interaction assay

Human WT SOD1 and SOD1G93A and mouse ATP1A3 nucleotide-binding domain (N, 372–586) were cloned into pOPINF [6] using the In-Fusion method (Clontech Laboratories Inc). Constructs were transformed into BL21 DE3 cells and proteins expressed via auto-induction at 20 °C for 20 h.

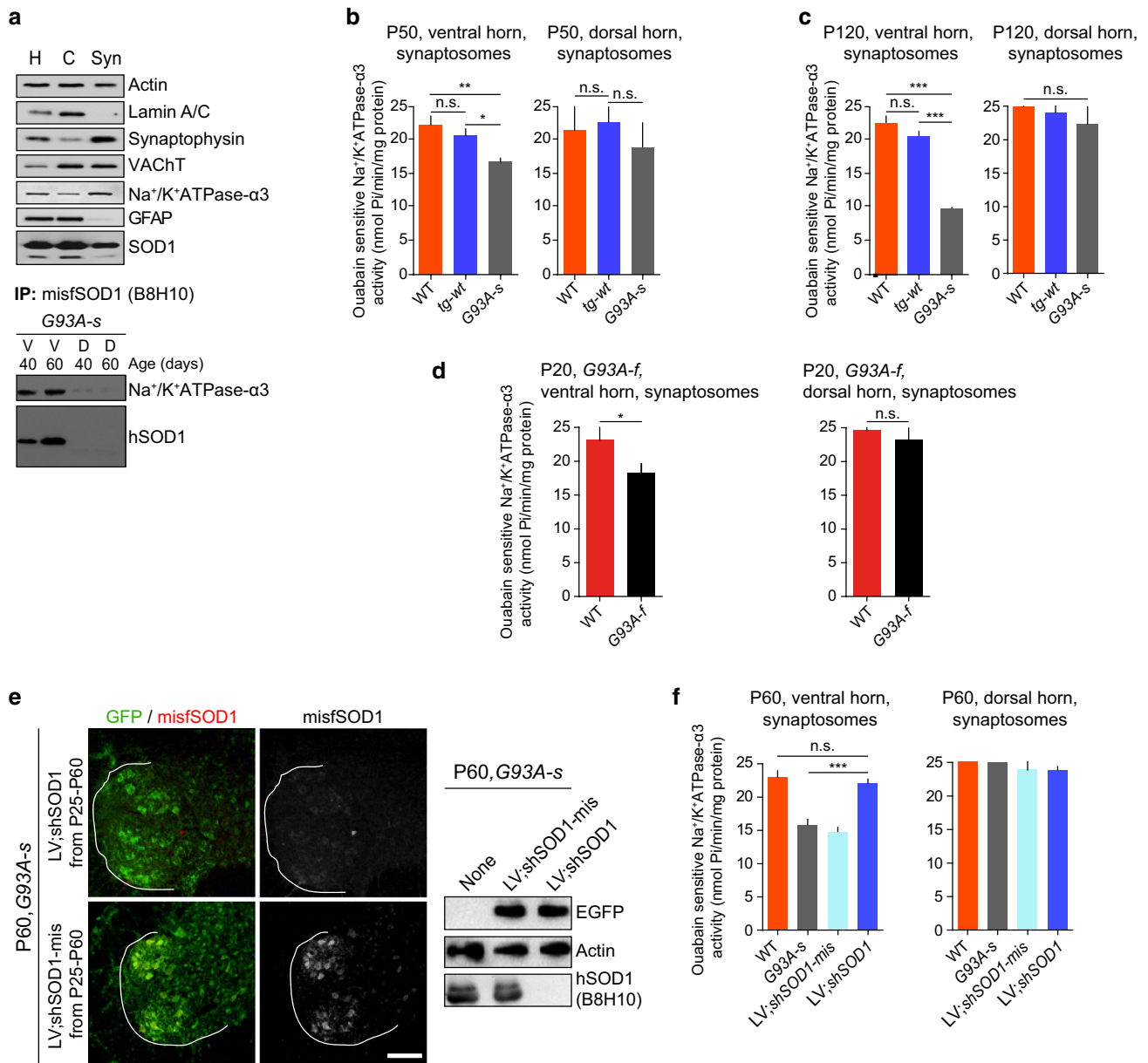


**Fig. 2** Early and selective impairment of Na<sup>+</sup>/K<sup>+</sup>ATPase-α3 activity in SOD1G93A mice. **a** Characterization of synaptosomes via IB for synaptic and non-synaptic markers. *H* homogenate, *C* cytoplasmic, *Syn* synaptosomal extract. Lack of nuclear marker Lamin A/C or astrocytic marker GFAP in synaptophysin enriched *Syn* extracts. *Bottom* co-IP with B8H10 from P40 and P60, *G93A-s* ventral horn (V) and dorsal horn (D) synaptosomes. IB for Na<sup>+</sup>/K<sup>+</sup>ATPase-α3 and SOD1 reveals the presence of misfSOD1 in association with Na<sup>+</sup>/K<sup>+</sup>ATPase-α3 in ventral horn synaptosomes. **b** Ouabain sensitive Na<sup>+</sup>/K<sup>+</sup>ATPase-α3 activity measured at P50 from WT, *G93A-s* and *tg-wt* ventral, dorsal horn synaptosomes reveals early impairment in Na<sup>+</sup>/K<sup>+</sup>ATPase-α3 activity in spinal ventral but not in dorsal horn of *G93A-s* mice. Values for activity represent the mean ± SEM for an average of 4 experiments, 4 mice/genotype. Ventral: \*\**p* = 0.0094, *F*<sub>(2,9)</sub> = 8.199 by ANOVA, \**p* < 0.05, \*\**p* < 0.01 post-ANOVA Tukey's test. Dorsal: *p* = 0.1158, *F*<sub>(2,9)</sub> = 2.766 by ANOVA. **c** Ouabain sensitive Na<sup>+</sup>/K<sup>+</sup>ATPase-α3 activity measured in P120, WT, *G93A-s* and *tg-wt* presents a decline by 50 % in Na<sup>+</sup>/K<sup>+</sup>ATPase-α3 activity from *G93A-s* ventral horn. Ventral: \*\*\**p* < 0.0001, *F*<sub>(2,9)</sub> = 58.12 by

ANOVA, \*\*\**p* < 0.001 for both comparisons by post-ANOVA Tukey's test. Dorsal: *p* = 0.5551, *F*<sub>(2,9)</sub> = 0.6289. *n* = 4 experiments, 4 mice/genotype, mean ± SEM. **d** Na<sup>+</sup>/K<sup>+</sup>ATPase-α3 activity measured in P20, *G93A-f* ventral horn reveals a significant reduction in activity compared to WT. Ventral horn: \**p* = 0.0230, unpaired *t* test, *t*(4) = 3.589, dorsal horn: *p* = 0.5480, unpaired *t* test, *t*(4) = 0.6555. Data are presented as mean ± SEM for an average of 3 experiments, 4 mice/genotype. **e** Lentiviral mediated knock down of hSOD1G93A in *G93A-s* mice. Representative image panel showing the transduction of MNs with GFP-tagged LV;shSOD1 or with mismatch shRNA (LV;shSOD1-mis). Scale 100 μm. Immunolabeling for misfSOD1 with B8H10 antibody shows successful knock down of SOD1G93A in LV;shSOD1 but not in LV;shSOD1-mis condition, confirmed by IB. **f** Measurement of Ouabain sensitive Na<sup>+</sup>/K<sup>+</sup>ATPase-α3 activity at P60 after knock down of SOD1 improves the observed deficit in activity. Values for activity represent the mean ± SEM for an average of 4 experiments, 4 mice/genotype. Ventral: \*\*\**p* < 0.0001, *F*<sub>(3,12)</sub> = 29.17 by ANOVA, \*\*\**p* < 0.001, by post-ANOVA Tukey's test. Dorsal: *p* = 0.0518, *F*<sub>(3,12)</sub> = 3.442 by ANOVA

Cells were harvested, resuspended in lysis buffer (50 mM Tris, pH 7.5, 500 mM NaCl, 20 mM imidazole, 0.2 % Tween-20) and frozen at  $-80^{\circ}\text{C}$ . Cell suspensions were thawed, freshly supplemented with Complete EDTA-free protease inhibitors (Roche Diagnostics) and 3 U/ml Benzozonase (Sigma) before passing through an Avestin Emulsi-Flex-C3 cell disruptor. For wt SOD1 and AT1A3 N-domain, clarified lysates were incubated with NiNTA affinity resin (Qiagen) in batch mode followed by cleavage of the  $6\times$  His-tag by addition of 3C protease and elution in 50 mM Tris, pH 7.5, 500 mM NaCl, 20 mM imidazole. Proteins were fractionated on a Superdex 75 HiLoad 16/60 (GE Healthcare) gel filtration column in GF buffer (20 mM Tris, pH 7.5, 200 mM NaCl, 2 mM TCEP (only used for AT1A3 N-domain) and 0.02 %  $\text{NaN}_3$ ). Peak fractions were pooled and concentrated to 9.7 (wt SOD1) and 6.0 mg/ml (AT1A3 N). For SOD1 G93A, clarified lysates were incubated with NiNTA affinity resin (Qiagen) in batch mode and the protein eluted in 50 mM Tris, pH 7.5, 500 mM NaCl, 125 mM imidazole and digested overnight at  $4^{\circ}\text{C}$  with 3C protease to remove the N-terminal histidine tag. The released protein tag and 3C protease were removed by a second nickel-affinity step and untagged SOD1 G93A was further purified over a Superdex 75 column in GF buffer and concentrated to 1.43 mg/ml. For ATP1A3 His-N, clarified lysates were incubated with NiNTA affinity resin (Qiagen) in batch mode and the protein eluted in 50 mM Tris, pH 7.5, 500 mM NaCl, 125 mM imidazole, followed by fractionation on a Superdex 75 HiLoad 16/60 (GE Healthcare) gel filtration column in GF buffer. Peak fractions were pooled and concentrated to 12.3 mg/ml. All proteins were stored at  $-80^{\circ}\text{C}$ . 10  $\mu\text{g}$  of purified His-N in 400  $\mu\text{l}$  of His-purification buffer (50 mM  $\text{NaH}_2\text{PO}_4\text{H}_2\text{O}$ , 300 mM NaCl, 20 mM imidazole) were incubated together with 25  $\mu\text{l}$  of nickel beads (Ni-NTA Magnetic Agarose Beads, Qiagen) for 1 h at  $4^{\circ}\text{C}$ . Beads were then washed  $3\times$  with His-purification buffer and resuspended in fresh 400  $\mu\text{l}$  of His-purification buffer containing either 1.5  $\mu\text{g}$  of purified WT-hSOD1 or 1.5  $\mu\text{g}$  of purified SOD1G93A and incubated for 1 h at  $4^{\circ}\text{C}$ , followed by washing  $4\times$  with His-purification buffer and eluted using His-tag elution buffer (50 mM  $\text{NaH}_2\text{PO}_4\text{H}_2\text{O}$ , 300 mM NaCl, 250 mM imidazole). Eluents were boiled with  $2\times$  loading buffer and then separated using 15 % SDS gel.

### Cell culture, transfection and protein extracts

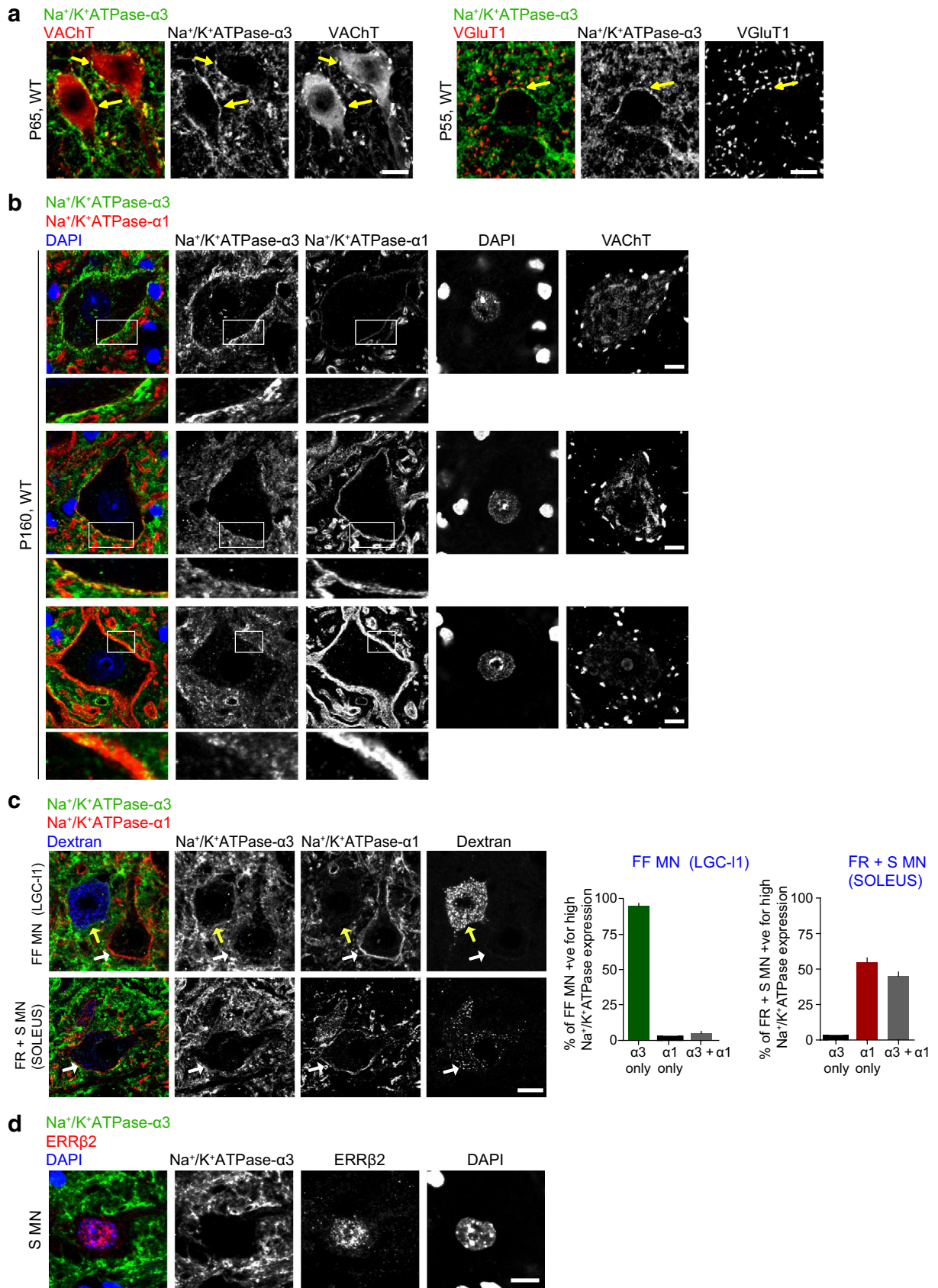
Mouse neuroblastoma cells (n2a) from (ATCC<sup>®</sup> CCL-131<sup>TM</sup>), mycoplasma tested were transiently transfected using TransIT-Neural (Mirus) or FuGENE HD transfection reagent (Promega) according to manufacturer's protocol. 36 h post transfection, cells were harvested and lysed in TNG-T lysis buffer (50 mM Tris-HCl pH 7.4, 100 mM NaCl, 10 % glycerol, 1 % Triton X-100, and proteinase inhibitor).

### Immunocytochemistry and antibodies

Mice were perfused with 4 % PFA in PBS, (L3–L5) lumbar spinal cord isolated and kept overnight at  $4^{\circ}\text{C}$  in 30 % sucrose. After embedding, 50  $\mu\text{m}$  cryostat sections were post fixed with 4 % PFA for 10 min, followed by PBS washes. Antibodies used for immunocytochemistry were: mouse anti-B8H10, 1:200 (Mediabs), rabbit anti- $\text{Na}^+/\text{K}^+$ ATPase- $\alpha_3$ , 1:200–500 (Abcam), goat anti- $\text{Na}^+/\text{K}^+$ ATPase- $\alpha_3$ , 1:200 (Santa Cruz), mouse anti- $\text{Na}^+/\text{K}^+$ ATPase- $\alpha_3$ , 1:200 (GeneTex),  $\alpha_6\text{F}$  monoclonal for  $\text{Na}^+/\text{K}^+$ ATPase- $\alpha_1$ , (1:100) developed by Douglas M. Fambrough and obtained from the Developmental Studies Hybridoma Bank, rabbit anti-BiP (ab21685), 1:500 (Abcam), mouse anti-KDEL Grp78, Grp94 (BiP), 1:1000 (Stressgen), rabbit anti-VACHT, 1:1000 (Chemicon), goat anti-VACHT (ab69000), 1:1000 (Abcam), goat anti-ChAT, 1:500 (Chemicon), rabbit anti-SOD1, 1:500 (Sigma), rabbit anti-GFP, 1:500 (Cell Signaling), mouse anti-Glutamate Receptor 2 (MAB397), 1:200 (Millipore), rabbit anti-GluA3 (AGC-010), 1:50 (Alomone labs), rabbit anti-Chondrolectin, 1:100 (Novus Biologicals), rabbit anti-VGluT1, 1:1000 (SYnaptic SYstems), mouse anti-ERR $\beta_2$ , 1:500 (R&D Systems), rabbit anti-NF-200, 1:200 (Abcam), rabbit anti-Synaptophysin, 1:500 (DAKO). Antibodies were applied in PBS-3 % BSA-0.3 % Triton-X 100, and incubated either overnight or for 3 days at  $4^{\circ}\text{C}$ . Sections were briefly washed with PBS and incubated for 4 h at RT with appropriate combinations of Alexa fluor-conjugated secondary antibodies (Invitrogen).

### Imaging and image analyses

Confocal images were acquired using a Leica SP5 (Leica Microsystems), fitted with  $20\times$  air objective, Olympus Fluoview 1000-BX61 (Olympus, Tokyo) microscope, fitted with  $20\times$  air objective or  $60\times$  Silicone oil objective. Images were processed using Imaris 7.6. For C-bouton volume, images were acquired with a Z-step size of 0.25  $\mu\text{m}$ . Imaris was used to build the isosurface of MNs present on the same plane and a volume was calculated for each C-bouton, which was plotted using GraphPad Prism 4. The analysis of BiP or misfSOD1 labeling intensities were performed as previously described [56, 58]. The extent of colocalization of two labels was measured using the “Colocalization” module of Imaris 7.6, 64-bit version (Bitplane AG, <http://www.bitplane.com>). The intensity of each label of the entire confocal stack was measured [11] to determine an intensity threshold for each of the two labels. Voxels with intensities above this threshold were considered to be above background. To avoid investigator bias in setting the thresholds, an automatic thresholding was used [11]. The extent of colocalization was calculated as “Percentage





◀ **Fig. 3** MN subtype specific expression of Na<sup>+</sup>/K<sup>+</sup>ATPase- $\alpha$ 1 and  $\alpha$ 3. **a** Immunolabeling of MNs with VAcHT (MN marker) and Na<sup>+</sup>/K<sup>+</sup>ATPase- $\alpha$ 3 reveals surface labeling outlining the MN soma (arrows) and dendrites. *Right* immunostaining of alpha-MN possessing VGLUT1 positive synaptic inputs and Na<sup>+</sup>/K<sup>+</sup>ATPase- $\alpha$ 3 reveals prominent surface labeling for Na<sup>+</sup>/K<sup>+</sup>ATPase- $\alpha$ 3. **b** Immunolabeling of WT spinal cord for VAcHT, Na<sup>+</sup>/K<sup>+</sup>ATPase- $\alpha$ 3 and  $\alpha$ 1 reveals differential expression pattern of the two Na<sup>+</sup>/K<sup>+</sup>ATPase isoforms. *Upper and lower panels* show representative example of a MN expressing strongly either Na<sup>+</sup>/K<sup>+</sup>ATPase- $\alpha$ 3 or  $\alpha$ 1. *Middle panel* presents a MN expressing both Na<sup>+</sup>/K<sup>+</sup>ATPase- $\alpha$ 3 and  $\alpha$ 1 isozymes. **c** Retrograde labeling of MN subtypes with Rhodamine dextran, immunolabeling for Na<sup>+</sup>/K<sup>+</sup>ATPase- $\alpha$ 3 and  $\alpha$ 1. *Right* Quantitative analyses (Q.A.) of % of alpha-MN subtypes expressing high levels of Na<sup>+</sup>/K<sup>+</sup>ATPase- $\alpha$ 3 and/or  $\alpha$ 1. Note the exclusive expression of Na<sup>+</sup>/K<sup>+</sup>ATPase- $\alpha$ 3 in FF MNs. **d** Slow MNs immunolabeled for S MN marker ERR $\beta$ 2 and Na<sup>+</sup>/K<sup>+</sup>ATPase- $\alpha$ 3 reveals that ERR $\beta$ 2 positive S MNs present negligible expression of Na<sup>+</sup>/K<sup>+</sup>ATPase- $\alpha$ 3. *Scale a* 20; *b, c, d* 10  $\mu$ m

of voxels above threshold in label “A” colocalized with respect to the second label B”.

### Purified microsomal fractions enriched in ER membranes

Microsomal fractions rich in ER membranes were isolated from the mouse ventral horn spinal cord as described previously [45]. Additional antibodies used for IB were rabbit anti-BiP (ab21685), 1:500–1000 (Abcam), mouse anti-Calnexin, 1:1000 (Millipore).

### Lentiviral vectors, generation and surgery

Replication-deficient, self-inactivating lentiviral (SIN) vectors pCCL-cPPT-PGK-EGFP-WPRE-LTR-H1-shRNA (LV;shSOD1 and LV;shSOD1-mis) generated by Patrick Aebischer laboratory [54] were ordered from Addgene (plasmid 10880 and 10881). Vesicular stomatitis virus G (VSV-G)-pseudotyped lentiviruses were produced by the transient calcium phosphate co-transfection of 293T cells. Na<sup>+</sup>/K<sup>+</sup>ATPase- $\alpha$ 3 encoding lentivirus was from GeneCopoeia, (Catalog #: LPP-OL05865-Lx304-050-S Lot #: GC08252K1413). Briefly mice were anaesthetized and laminectomy was performed as described [32, 54]. Lentiviral vectors  $1 \times 10^6$  or  $10^7$  transduction units (TU) were bilaterally injected using a 5- $\mu$ l Hamilton syringe with a 34-gauge needle at two sites separated by 2 mm in the lumbar L3–L4 region using a stereotaxic frame.

### AAV6 Na<sup>+</sup>/K<sup>+</sup>ATPase- $\alpha$ 3-swap loop generation and injection

The Na<sup>+</sup>/K<sup>+</sup>ATPase- $\alpha$ 3-swap loop construct was used to produce serotype 6 AAV particles (AAV2/6) by ViroVeK

(Hayward, CA, USA). Injection of AAV particles in neonatal mice (P0–P2) was performed by unilateral injection of 3  $\mu$ l of  $2.6 \times 10^{11}$  VG in the lateral ventricle, as described previously [14]. A 0.04 % fast green solution was added to the vector suspension in order to visualize the spread of the vector suspension in the ventricular system. AAV6-GFP was provided to us by Patrick Aebischer, EPFL, Lausanne, Switzerland.

### Measurement of muscle strength and survival

Muscle strength was measured using the grid test as previously described [56]. All mice were naive, trained for 3 days prior to the start of the experiment. Measurements were done blindly without knowing the genotype of the mice. To measure longevity, survival of mice was followed up to a point when mice could no longer right themselves within 20 s after being put on the side. Kaplan–Meier survival curves were made using GraphPad Prism 6 Software, and significance was calculated using Log-rank test.

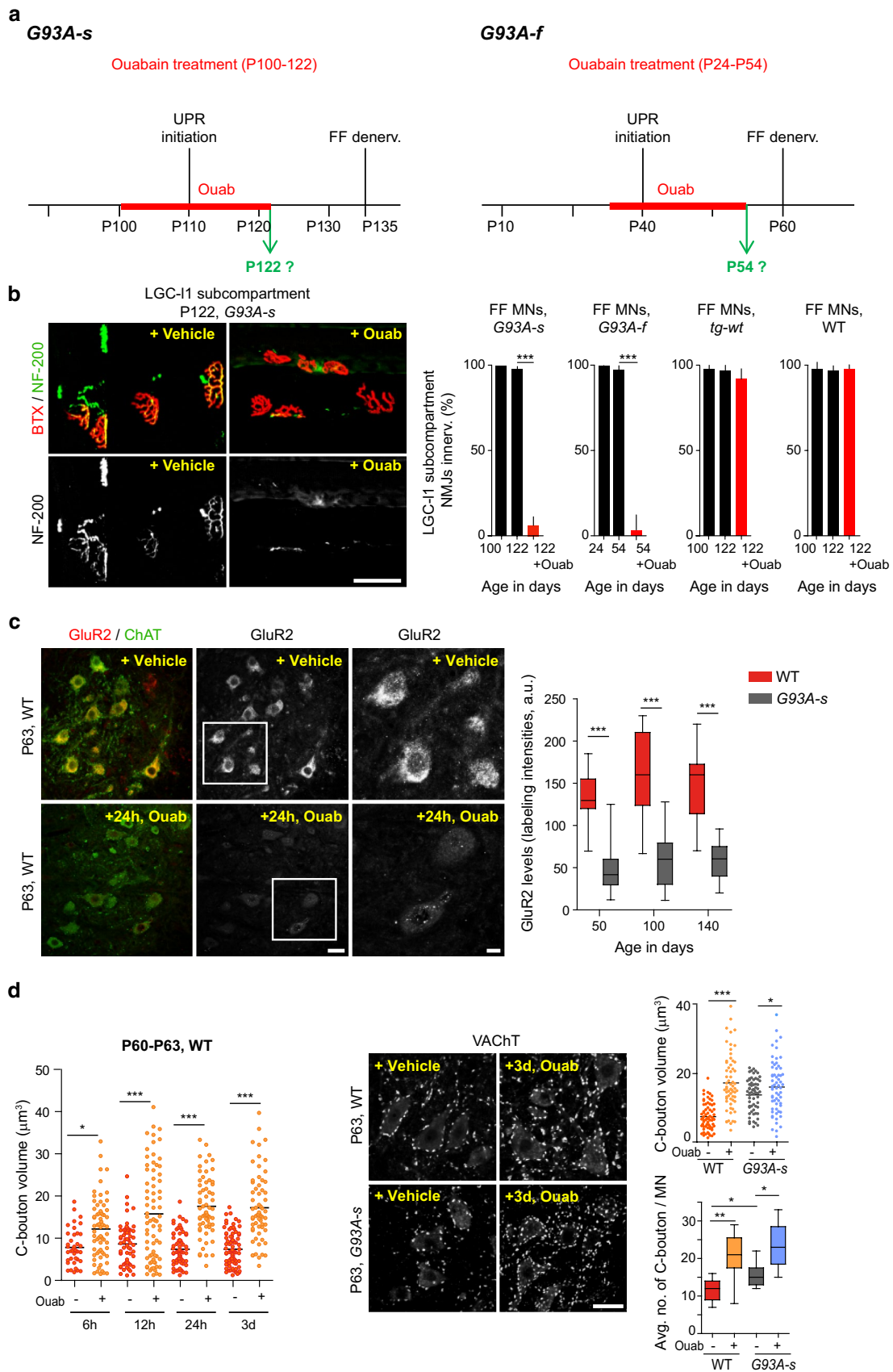
### Statistical analysis

For immuno-quantification experiments, differences were evaluated for their statistical significance by two-tailed, unpaired Student’s *t* test to compare two groups and ANOVA to compare three or more groups. Post-ANOVA Tukey’s test was used to evaluate statistical significance throughout the paper. Values were expressed as mean or mean  $\pm$  standard error of the mean (SEM). \**p* < 0.05, \*\**p* < 0.01, \*\*\**p* < 0.001.

## Results

### Mapping the misfSOD1 interactome with conformation specific antibody B8H10

A portion of mutSOD1 exists in a non-native or misfolded conformation in MNs in the spinal cord. To determine the aberrant interactome of misfSOD1, we used the conformation specific antibody B8H10 and co-immunoprecipitated (co-IP) misfSOD1 from the ventral horn of medium expresser transgenic mice; SOD1G93A-slow (*G93A-s*) and wild-type (WT) mice at three ages: P15 (earliest detection of disease epitope B8H10 in disease vulnerable FF MNs), P50 (early presymptomatic stage) and P100 (presymptomatic stage, 30–35 days before disconnection of FF axons from the muscle fibers). To avoid detection of secondary interactions associated with UPR, mitochondrial and proteasomal dysfunctions, mass spectrometric (MS) analyses was performed at a very early age of P15 in *G93A-s* mice. MS analyses of the immunoprecipitates identified



◀ **Fig. 4** Inhibition of Na<sup>+</sup>/K<sup>+</sup>ATPase- $\alpha$ 3 pump anticipates disease and modulates synaptic connectivity onto MNs. **a** Schematic of the experiments performed on *G93A-s* and *G93A-f* mice described in the figure. Bars indicate durations of the Ouabain (Ouab) treatments; colored downwards arrows indicate ages at which mice were analyzed. Vertical bars indicate UPR initiations and FF denervations (FF denerv.) ages. **b** Ouabain treatment anticipates disease manifestation. Analysis of the LGC-11 muscle subcompartment innervated by FF MNs at P54, *G93A-f* (6 days before FF MNs denervate in *G93A-f* mice) and at P122, *G93A-s* (10–13 days before FF axons disconnect in *G93A-s* mice), reveals premature MN denervation after Ouabain treatment. Representative image showing loss of Neurofilament (NF) staining in treated *G93A-s* mice. Q.A. of denervated NMJs in the LGC-11 subcompartment after Ouabain treatment in *G93A-s* and *G93A-f* mice but not in control WT and *tg-wt* condition. Data are presented as mean  $\pm$  SEM, *G93A-s*: \*\*\* $p$  < 0.0001,  $F_{(2,9)} = 935.4$  by ANOVA, \*\*\* $p$  < 0.001 by post-ANOVA Tukey's test,  $n = 4$  mice each condition. *G93A-f*: \*\*\* $p$  < 0.0001,  $F_{(2,6)} = 234.1$  by ANOVA, \*\*\* $p$  < 0.001 by post-ANOVA Tukey's test,  $n = 3$  mice each condition. **c** Inhibiting Na<sup>+</sup>/K<sup>+</sup>ATPase- $\alpha$ 3 functioning via Ouabain for 24 h in WT spinal cord leads to loss of Glutamate receptor 2 (GluR2) immunoreactivity in MNs. Boxed are zoom in: MN with GluR2 labeling +/- Ouabain. Right reduced expression of GluR2 in *G93A-s* mice over disease, Q.A. of GluR2 intensity (\*\*\* $p$  < 0.0001,  $F_{(5,144)} = 58.26$  by ANOVA, \*\*\* $p$  < 0.001 by post-ANOVA Tukey's test,  $n = 24$ –26 MNs/condition from 3 mice). **d** Acutely blocking Na<sup>+</sup>/K<sup>+</sup>ATPase- $\alpha$ 3 leads to an increase in size of cholinergic synapses (C-boutons) on WT MNs. Immunolabeling for C-boutons (VAcHT) after 6 h, 12 h, 24 h or 3 days of Ouabain treatment in WT mice reveals altered C-bouton morphology. Q.A. of C-bouton volume, (\*\*\* $p$  < 0.0001,  $F_{(7,498)} = 26.98$ , by ANOVA, \* $p$  < 0.05, \*\*\* $p$  < 0.001 by post-ANOVA Tukey's test,  $n = 39$ –75 C-boutons). Right comparison of C-bouton volume between WT and *G93A-s* MNs after +/- 3 days Ouabain. Q.A. of C-bouton volume (\*\*\* $p$  < 0.0001,  $F_{(3,252)} = 32.32$  by ANOVA, \* $p$  < 0.05, \*\*\* $p$  < 0.001 in post-ANOVA Tukey's test,  $n = 62$ –68 C-boutons from 4 mice each condition) and C-bouton density on to MN soma (\*\*\* $p$  = 0.0003,  $F_{(3,28)} = 8.622$  by ANOVA, \* $p$  < 0.05, \*\* $p$  < 0.01 in post-ANOVA Tukey's test,  $n = 8$  sections from 3 mice for all genotypes) indicates an increase in volume as well as numbers of C-boutons after Ouabain treatment. Scale **b** 50, **c** 20, zoom 10, **d** 20  $\mu$ m

24 proteins at P15, 19 proteins at P50 and 31 proteins at P100, which were in a complex with misfSOD1 and were absent in WT immunoprecipitates. Of these interacting proteins, five were shared between all three ages and ten were shared between P50 and P100 (Fig. 1a, and Suppl. Table 1 for complete list of proteins). PANTHER (Protein ANalysis THrough Evolutionary Relationships) analysis of the misfSOD1 interactome revealed that B8H10 specific misfSOD1 interactions comprised mainly proteins belonging to chaperones, transporters and hydrolases protein classes (Fig. 1a). Additionally, misfSOD1 interactions involved clusters of proteins belonging to the same family and sharing a high degree of structural homology, suggesting that these associations were non-random. Moreover, functional analyses revealed a selective enrichment of proteins possessing an ATPase activity and accounting for ion transport functions (Suppl. Fig. 1a–b). Of the five shared misfSOD1 interacting proteins, chaperone Heat shock cognate 71 kDa protein (HSPA8), Na<sup>+</sup>/K<sup>+</sup>ATPase- $\alpha$ 3 and adaptor protein 14-3-3 protein gamma exhibited an age dependent

two-fold or more increase in abundance as measured semi quantitatively via peptide match score summation (PMSS) (Fig. 1b–c). This suggested that these aberrant interactions were specific as their association with misfSOD1 increased in parallel to the increase in age dependent accumulation of misfSOD1 in MNs (Suppl. Fig. 1c). To further confirm visually the specificity of our finding, anti-B8H10 co-IP were run on SDS-page gels, silver stained and individual bands for Na<sup>+</sup>/K<sup>+</sup>ATPase- $\alpha$ 3, HSPA8 and misfSOD1 were analyzed via MS (Suppl. Fig. 1d).

Besides chaperone HSPA8 and 14-3-3 gamma, the association of misfSOD1 with Na<sup>+</sup>/K<sup>+</sup>ATPase- $\alpha$ 3 was detected at P15 which coincided in time with the earliest recorded alterations in MN excitability in mutSOD1 models, including the *G93A-s* mice [46]. As Na<sup>+</sup>/K<sup>+</sup>ATPase- $\alpha$ 3 is exclusively neuronal [30, 42], critically involved in the maintenance of neuronal membrane potential and its expression levels as well as pump activity is increased as a function of neuronal activity [23], we focused the study on the complex consisting of misfSOD1 and Na<sup>+</sup>/K<sup>+</sup>ATPase- $\alpha$ 3. Co-IP of misfSOD1 via B8H10 from *G93A-s* spinal cord and immunoblotting (IB) for Na<sup>+</sup>/K<sup>+</sup>ATPase- $\alpha$ 3 confirmed an interaction between misfSOD1 and Na<sup>+</sup>/K<sup>+</sup>ATPase- $\alpha$ 3 as from P15, which increased with increasing accumulation of misfSOD1 (Fig. 1d). As control for the specificity of the interaction, co-IP with mouse IgG followed by IB with B8H10 revealed no unspecific association of mutSOD1 with mouse IgG (Fig. 1e). To distinguish between aberrant versus normal interaction, co-IP of Na<sup>+</sup>/K<sup>+</sup>ATPase- $\alpha$ 3 from protein lysates of transgenic mice overexpressing WT human SOD1 (*tg-wt*), WT and *G93A-s* mice was performed, which confirmed that the interaction of Na<sup>+</sup>/K<sup>+</sup>ATPase- $\alpha$ 3 with misfSOD1 was due to a mutation in hSOD1 as this interaction was not detected in WT nor in *tg-wt* mice (Fig. 1f). As additional evidence, co-IP experiments from a different SOD1 model; SOD1G37R (*G37R*) presented the existence of a misfSOD1-Na<sup>+</sup>/K<sup>+</sup>ATPase- $\alpha$ 3 complex (Fig. 1g). Neurons in the ventral horn express both Na<sup>+</sup>/K<sup>+</sup>ATPase- $\alpha$ 1 and  $\alpha$ 3 isozymes sharing a high degree of sequence identity [42]. Therefore, to pin down the specificity of the interaction, Na<sup>+</sup>/K<sup>+</sup>ATPase- $\alpha$ 1 was immunoprecipitated from WT and *G93A-s* spinal protein lysates, which revealed no interaction with SOD1 at P100 (Fig. 1h).

### Early impairment in Na<sup>+</sup>/K<sup>+</sup>ATPase- $\alpha$ 3 activity in the ventral horn of the spinal cord

We examined whether the existence of an aberrant complex between misfSOD1 and Na<sup>+</sup>/K<sup>+</sup>ATPase- $\alpha$ 3 would impact the physiological functioning of the Na<sup>+</sup>/K<sup>+</sup>ATPase- $\alpha$ 3 pump. To this end, Na<sup>+</sup>/K<sup>+</sup>ATPase- $\alpha$ 3 activity was measured from purified synaptosomes isolated from the ventral and the dorsal horn of the spinal cord from WT, *tg-wt* and



*G93A-s* mice. Along with biochemical characterization of synaptosome purity via enrichment of synaptic proteins, the presence of misfSOD1 and Na<sup>+</sup>/K<sup>+</sup>ATPase- $\alpha$ 3 complex in the ventral horn synaptosomes was verified (Fig. 2a). Measurement of Na<sup>+</sup>/K<sup>+</sup>ATPase- $\alpha$ 3 activity from P50, *G93A-s* ventral horn synaptosomes revealed a significant reduction of 25 % compared to WT. Moreover, Na<sup>+</sup>/K<sup>+</sup>ATPase- $\alpha$ 3 activity in *G93A-s* was reduced by 18.5 % compared to *tg-wt*, suggesting that this impairment was not due to the sole overexpression of hSOD1 protein (Fig. 2b). In contrast, dorsal horn synaptosomes exhibited no significant changes in Na<sup>+</sup>/K<sup>+</sup>ATPase- $\alpha$ 3 activity and early functional impairment in Na<sup>+</sup>/K<sup>+</sup>ATPase- $\alpha$ 3 activity was restricted to spinal regions harboring MNs. Measuring Na<sup>+</sup>/K<sup>+</sup>ATPase- $\alpha$ 3 activity at P120, a time point coinciding with the appearance of UPR; an early cellular event in disease vulnerable FF MNs, presented a strong reduction of 56 % in Na<sup>+</sup>/K<sup>+</sup>ATPase- $\alpha$ 3 activity in *G93A-s* compared to WT and 52 % compared to *tg-wt* (Fig. 2c). Similar measurements performed on high expresser transgenic mice; SOD1*G93A-fast* (*G93A-f*) revealed altered Na<sup>+</sup>/K<sup>+</sup>ATPase- $\alpha$ 3 activity in the ventral but not dorsal regions of the spinal cord as early as P20 (Fig. 2d). To validate the involvement of mutSOD1 for the observed impairment in Na<sup>+</sup>/K<sup>+</sup>ATPase- $\alpha$ 3 activity, a lentiviral mediated knock down of mutSOD1 via shRNA (LV;shSOD1) at P25 was performed and 35 days later Na<sup>+</sup>/K<sup>+</sup>ATPase- $\alpha$ 3 activity was measured (Fig. 2e). The reduction in mutSOD1 expression rescued Na<sup>+</sup>/K<sup>+</sup>ATPase- $\alpha$ 3 activity to WT levels, demonstrating that mutSOD1 expression was needed for the observed early functional impairment of Na<sup>+</sup>/K<sup>+</sup>ATPase- $\alpha$ 3 activity (Fig. 2f).

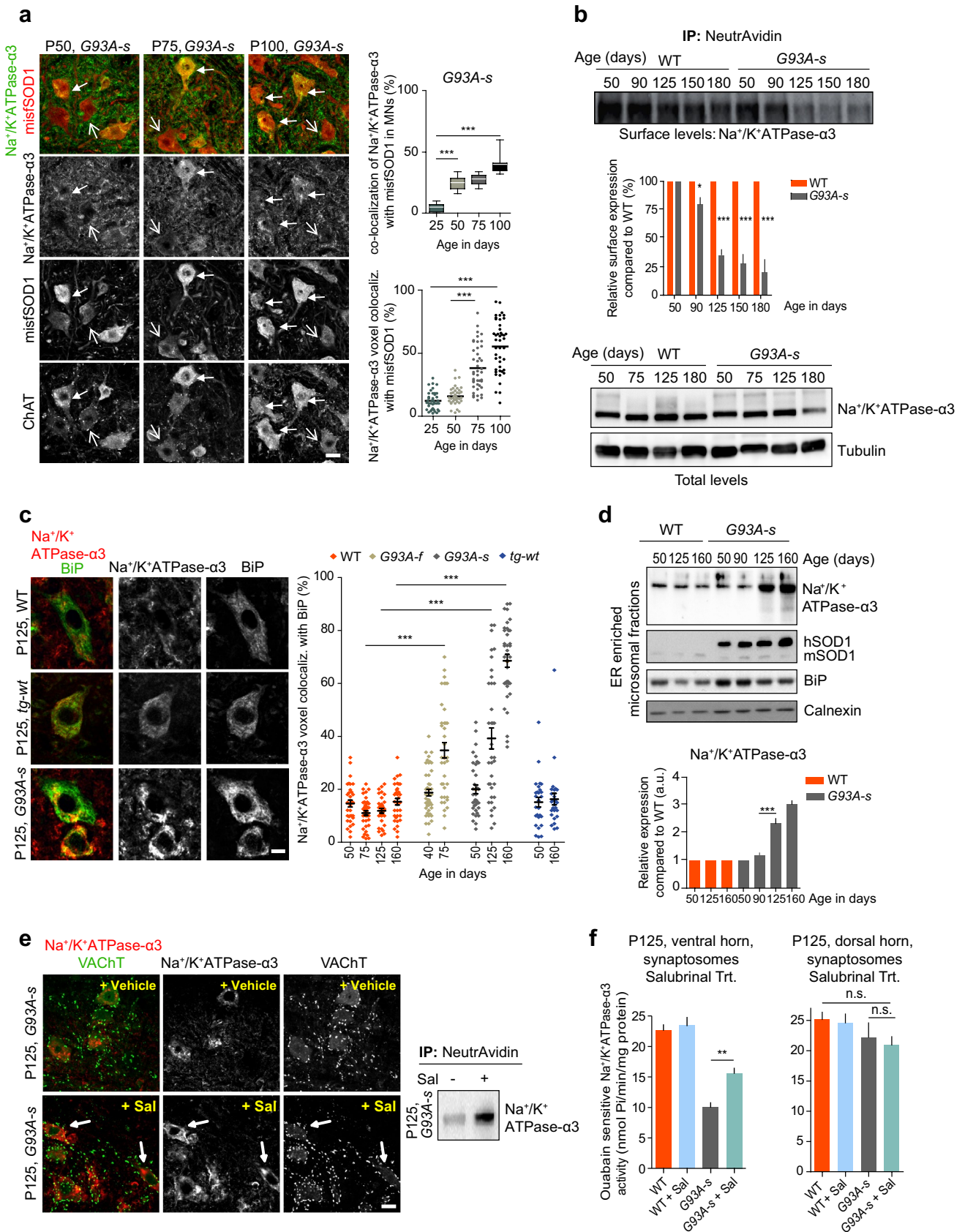
### Na<sup>+</sup>/K<sup>+</sup>ATPase- $\alpha$ 3 is highly expressed in vulnerable FF MNs

Since misfSOD1 appears first in a fraction of vulnerable MNs and forms a complex with Na<sup>+</sup>/K<sup>+</sup>ATPase- $\alpha$ 3 but not with Na<sup>+</sup>/K<sup>+</sup>ATPase- $\alpha$ 1, we examined the expression pattern of Na<sup>+</sup>/K<sup>+</sup>ATPase- $\alpha$ 3 and  $\alpha$ 1 in MNs. Immunolabeling revealed that Choline acetyl transferase (ChAT) positive WT MNs expressed Na<sup>+</sup>/K<sup>+</sup>ATPase- $\alpha$ 3 on the surface of MN soma and concentrated along dendrites, juxtaposed with C-boutons (the presynaptic ending of cholinergic partition cells) or with vesicular glutamate transporter 1 (VGluT1, the proprioceptive terminal on MNs) in the ventral horn of the spinal cord (Fig. 3a). Further, a population of ChAT positive MNs presented high levels of Na<sup>+</sup>/K<sup>+</sup>ATPase- $\alpha$ 3 and low levels of  $\alpha$ 1 immunolabeling. In a second subpopulation of MNs, Na<sup>+</sup>/K<sup>+</sup>ATPase- $\alpha$ 3 and  $\alpha$ 1 expression at equal levels were observed. Lastly, a small group of MNs expressed primarily Na<sup>+</sup>/K<sup>+</sup>ATPase- $\alpha$ 1 (Fig. 3b). To examine whether this differential expression

**Fig. 5** Reduced surface expression of Na<sup>+</sup>/K<sup>+</sup>ATPase- $\alpha$ 3 in *G93A-s* MNs. **a** MisfSOD1 and Na<sup>+</sup>/K<sup>+</sup>ATPase- $\alpha$ 3 accumulate intracellularly in ChAT positive *G93A-s* MNs (closed arrows). MNs presenting no intracellular accumulation of Na<sup>+</sup>/K<sup>+</sup>ATPase- $\alpha$ 3 and a normal membrane labeling (open arrows). **Right** Q.A. mutant MNs (%) displaying intracellular colocalization of Na<sup>+</sup>/K<sup>+</sup>ATPase- $\alpha$ 3 with misfSOD1,  $n = 9$  sections from 4 mice/genotype,  $***p < 0.0001$ ,  $F_{(3,32)} = 59.62$  by ANOVA,  $***p < 0.001$  for both comparisons in post-ANOVA Tukey's test. **Bottom** Q.A. of % of voxel of Na<sup>+</sup>/K<sup>+</sup>ATPase- $\alpha$ 3 colocalized with misfSOD1,  $n = 40$ –44 MNs from 3 mice,  $***p < 0.0001$ ,  $F_{(3,163)} = 79.26$  by ANOVA,  $***p < 0.001$  for both comparisons by post-ANOVA Tukey's test. **b** **Top** surface biotinylation of WT and *G93A-s* spinal cord slices, IB: Na<sup>+</sup>/K<sup>+</sup>ATPase- $\alpha$ 3. Visible reduction of surface Na<sup>+</sup>/K<sup>+</sup>ATPase- $\alpha$ 3 in P125, *G93A-s*. **Middle** Q.A. relative surface values of Na<sup>+</sup>/K<sup>+</sup>ATPase- $\alpha$ 3 by comparing surface expression in WT for each age.  $n = 4$  experiments, mean  $\pm$  SEM,  $***p < 0.0001$ ,  $F_{(9,30)} = 365.5$  by ANOVA,  $*p < 0.05$ ,  $***p < 0.001$  by post-ANOVA Tukey's test. **Bottom** IB for total Na<sup>+</sup>/K<sup>+</sup>ATPase- $\alpha$ 3 and tubulin levels. Note the constant total Na<sup>+</sup>/K<sup>+</sup>ATPase- $\alpha$ 3 level in P125, *G93A-s* spinal cord despite reduction in surface levels at the same age. **c** Immunostaining of spinal sections for Na<sup>+</sup>/K<sup>+</sup>ATPase- $\alpha$ 3 and BiP, an ER marker. Na<sup>+</sup>/K<sup>+</sup>ATPase- $\alpha$ 3 colocalizes with BiP in the ER in mutant *G93A-s*, but not in WT and *tg-wt* MNs. Single plane images through the ER. **Right** Q.A. % of Na<sup>+</sup>/K<sup>+</sup>ATPase- $\alpha$ 3 voxels overlapping with BiP ( $n = 32$ –48 MNs from 3 mice/genotype,  $***p < 0.0001$ ,  $F_{(10,371)} = 69.18$  by ANOVA,  $***p < 0.001$  by post-ANOVA Tukey's test). **d** ER enriched microsomal fractions from ventral horns of the spinal cord. IB for Na<sup>+</sup>/K<sup>+</sup>ATPase- $\alpha$ 3, SOD1 and ER markers BiP and Calnexin. **Bottom** relative presence of Na<sup>+</sup>/K<sup>+</sup>ATPase- $\alpha$ 3 in the ER, plotted as mean  $\pm$  SEM by comparing ER values in *G93A-s* to WT,  $***p < 0.0001$ ,  $F_{(6,14)} = 89.68$  by ANOVA,  $***p < 0.001$  by post-ANOVA Tukey's test ( $n = 3$  experiments, 8 mice each age). **e** Immunolabeling for Na<sup>+</sup>/K<sup>+</sup>ATPase- $\alpha$ 3 and VAcHt  $\pm$  6 days of Salubrial (Sal) treatment (ER stress inhibitor) in *G93A-s* mice. Analysis done at P125, increased surface levels of Na<sup>+</sup>/K<sup>+</sup>ATPase- $\alpha$ 3 (white arrows) were observed in Salubrial treated MNs. **Right** surface biotinylation of *G93A-s* spinal cord sections after Salubrial treatment followed by IB for Na<sup>+</sup>/K<sup>+</sup>ATPase- $\alpha$ 3 reveals increased surface levels of Na<sup>+</sup>/K<sup>+</sup>ATPase- $\alpha$ 3 as compared to untreated condition. **f** Ouabain sensitive Na<sup>+</sup>/K<sup>+</sup>ATPase- $\alpha$ 3 activity measured at P125 after Salubrial treatment. The treatment inhibited ER stress and led to an increase of about 50 % in Na<sup>+</sup>/K<sup>+</sup>ATPase- $\alpha$ 3 activity in the ventral horn synaptosomes. Ventral:  $***p < 0.0001$ ,  $F_{(3,12)} = 42.43$ , dorsal:  $p = 0.3033$ ,  $F_{(3,12)} = 1.433$  by ANOVA,  $**p = 0.0025$ , post-ANOVA Tukey's test,  $n = 4$  experiments in case of ventral and 3 experiments in case of dorsal with 4 mice each condition. **Scale** **a**, **e** 20, **c** 10  $\mu$ m

of Na<sup>+</sup>/K<sup>+</sup>ATPase- $\alpha$ 3 and  $\alpha$ 1 was MN subtype dependent, retrograde labeling with rhodamine dextran was performed in WT mice, where vulnerable FF MNs were labeled from the lateral gastrocnemius sub-compartment 11 (LGC-11) or resistant FR+S MNs were labeled from the soleus muscle. Subsequent, immunostaining revealed that FF MNs predominantly express high levels of Na<sup>+</sup>/K<sup>+</sup>ATPase- $\alpha$ 3 whereas half of the soleus MNs co-expressed both Na<sup>+</sup>/K<sup>+</sup>ATPase- $\alpha$ 1 and Na<sup>+</sup>/K<sup>+</sup>ATPase- $\alpha$ 3 at almost equal levels and the other half mainly expressed Na<sup>+</sup>/K<sup>+</sup>ATPase- $\alpha$ 1 (Fig. 3c). To further delineate Na<sup>+</sup>/K<sup>+</sup>ATPase expression in the soleus MN pool, immunostaining with Estrogen related receptor beta (ERR $\beta$ ); a marker for S MNs in the spinal cord [17], was performed, revealing that ERR $\beta$  positive





S MNs express negligible amounts of Na<sup>+</sup>/K<sup>+</sup>ATPase- $\alpha$ 3 (Fig. 3d). This segregation in the expression of Na<sup>+</sup>/K<sup>+</sup>ATPase- $\alpha$ 3 and  $\alpha$ 1 is not unique to the spinal MNs but also observed in other neuronal populations in the CNS as previously described [42]. These experiments suggest that MNs show differential expression of Na<sup>+</sup>/K<sup>+</sup>ATPase- $\alpha$ 3 and  $\alpha$ 1, which might be indicative of their specialized role in contributing to the differential intrinsic excitability of MNs.

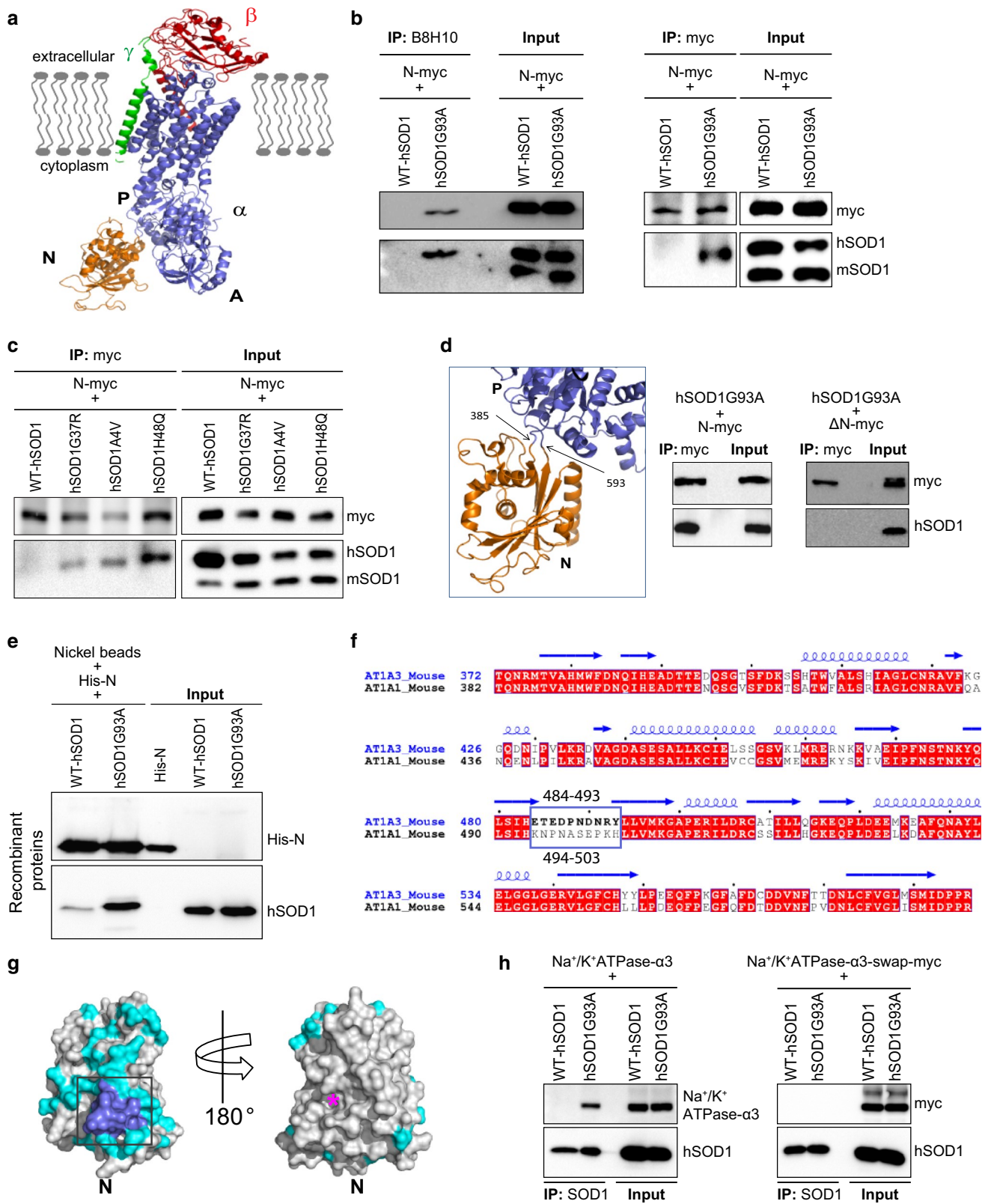
### Pharmacological inhibition of Na<sup>+</sup>/K<sup>+</sup>ATPase accelerates disease pathology

To determine whether the early impairment in Na<sup>+</sup>/K<sup>+</sup>ATPase- $\alpha$ 3 activity in MNs contributes to disease progression, presymptomatic *G93A-s*, *G93A-f*, *tg-wt* and WT mice were treated with the Na<sup>+</sup>/K<sup>+</sup>ATPase inhibitor Ouabain. Na<sup>+</sup>/K<sup>+</sup>ATPase- $\alpha$ 3 has the highest sensitivity to low concentrations of Ouabain (IC<sub>50</sub> values: 0.1–1  $\mu$ M for  $\alpha$ 3 and 32  $\mu$ M for  $\alpha$ 1) [37, 62]. Treatments with Ouabain were started before the onset of the earliest identifiable cellular dysfunction in MNs (i.e. UPR) and analyses of the neuromuscular junctions (NMJs) were performed 6–13 days before the first wave of nerve fiber degeneration (i.e. at P54 in *G93A-f*, or at P122 in *G93A-s* mice) (see scheme in Fig. 4a). Analysis of the NMJs in the treated animals revealed anticipated denervation of the target muscle fiber in the LGC-II sub-compartment, which is purely innervated by the most vulnerable FF MNs (Fig. 4b). Soleus muscle innervated by resistant FR and S MNs did not display signs of axonal disconnection from the muscle after Ouabain treatment (Suppl. Fig. 2a). Since FF MNs denervate synchronously and reproducibly in the hind limb muscles between P60 and P62 in *G93A-f* and between P135 and P137 in *G93A-s* mice, this anticipated denervation indicates that deficits in Na<sup>+</sup>/K<sup>+</sup>ATPase- $\alpha$ 3 activity might play a role in accelerating the pathology. Further, enhanced activation of astrocytes around MNs was observed in *G93A-s* spinal cord after Ouabain administration, highlighting anticipated disease pathology (Suppl. Fig. 2b). Chronic treatment led to a progressive decline in muscle strength in *G93A-f* mice and an overall decrease in life span of approximately 12 % in both mouse models of fALS (Suppl. Fig. 2c–d).

We assessed whether impairments in Na<sup>+</sup>/K<sup>+</sup>ATPase- $\alpha$ 3 activity could alter mechanisms associated with MN excitability. Ionotropic AMPA receptor 2 (GluR2) expression levels were strikingly reduced within WT MNs 24 h after intraspinal Ouabain administration. Quantifying GluR2 labeling intensities in *G93A-s* MNs revealed a significant and early reduction in GluR2 expression over disease course (Fig. 4c). Moreover, GluR3 subunit expression was increased after Ouabain application suggesting that alterations in Na<sup>+</sup>/K<sup>+</sup>ATPase- $\alpha$ 3 activity might influence the

**Fig. 6** Identification of the interaction site between misfSOD1 and Na<sup>+</sup>/K<sup>+</sup>ATPase- $\alpha$ 3. **a** Crystal structure of *S. acanthias* Na<sup>+</sup>/K<sup>+</sup>ATPase (PDB 2ZXE [60]) shown as a cartoon for  $\alpha$  (blue/orange),  $\beta$  (red), and  $\gamma$  (green) subunits. The cytosolic nucleotide-binding domain (N, orange), actuator domain (A, blue) and phosphorylation domain (P, blue) of the  $\alpha$ -subunit are labeled. **b** Co-IP with B8H10 antibody from n2a cells co-transfected with WT-hSOD1 or hSOD1G93A and myc-tagged nucleotide-binding domain (N-myc) of Na<sup>+</sup>/K<sup>+</sup>ATPase- $\alpha$ 3, IB: myc and SOD1 indicates that misfSOD1 interacts with N-myc. **Right** Reverse co-IP with myc antibody and IB for SOD1 and myc. **c** Detection of N-myc-mutSOD1 complex with different SOD1 mutations: hSOD1G37R, hSOD1A4V, hSOD1H48Q. **d** Zoom-in on the N-domain (orange) of *S. acanthias* Na<sup>+</sup>/K<sup>+</sup>ATPase- $\alpha$ 3 (2ZXE [60]), highlighting linking residues to the remaining  $\alpha$ -chain (blue). Deletion of residues 375–583 (orange) in mouse Na<sup>+</sup>/K<sup>+</sup>ATPase- $\alpha$ 3 (corresponding to residues 385–593 in 2ZXE) removes the N-domain without perturbing the fold of the rest of the protein. Co-IP with myc antibody from cells co-transfected with hSOD1G93A and N-myc or full length Na<sup>+</sup>/K<sup>+</sup>ATPase- $\alpha$ 3 lacking the N-domain [ $\Delta$ 375–583 ( $\Delta$ N-myc)] followed by IB with SOD1 and myc reveals loss of association of misfSOD1 with Na<sup>+</sup>/K<sup>+</sup>ATPase- $\alpha$ 3 lacking N-domain. **e** hSOD1G93A interacts directly with nucleotide-binding domain of Na<sup>+</sup>/K<sup>+</sup>ATPase- $\alpha$ 3. Purified recombinant N-domain of Na<sup>+</sup>/K<sup>+</sup>ATPase- $\alpha$ 3 with N-terminal His tag (His-N) was incubated together with WT-hSOD1 or hSOD1G93A. Complex bound to Nickel beads and eluted. IB for His-N via Na<sup>+</sup>/K<sup>+</sup>ATPase- $\alpha$ 3 and SOD1 revealed a direct interaction between SOD1G93A and His-N recombinant proteins. **f** Clustal Omega sequence alignment (<http://www.ebi.ac.uk/Tools/msa/clustalw2/>) of mouse Na<sup>+</sup>/K<sup>+</sup>ATPase- $\alpha$ 3 and  $\alpha$ 1 nucleotide-binding domains (N). Identical residues are boxed in red while the longest continuous stretch that differs between the two sequences (acidic loop) which has been swapped between N-domain of  $\alpha$ 3 to that of  $\alpha$ 1 is framed in blue. Secondary structure elements of the Na<sup>+</sup>/K<sup>+</sup>ATPase- $\alpha$ 3 N-domain are displayed in blue above the alignment. **g** Surface representation of mouse Na<sup>+</sup>/K<sup>+</sup>ATPase- $\alpha$ 3 N-domain homology model in two orientations rotated around a vertical axis by 180°. The homology model was created using the HHpred pipeline (<http://toolkit.tuebingen.mpg.de/hhpred>) with the N-domain of PDB 2ZXE (77 % sequence identity) as template. Residues differing between the N-domains of Na<sup>+</sup>/K<sup>+</sup>ATPase- $\alpha$ 3 and  $\alpha$ 1 are highlighted in cyan and blue. The acidic loop is in blue and highlighted in a black box. The nucleotide binding cleft is marked with an asterisk in magenta. **h** Co-IP with SOD1 from n2a cells co-transfected with WT-hSOD1 or hSOD1G93A and Na<sup>+</sup>/K<sup>+</sup>ATPase- $\alpha$ 3 or Na<sup>+</sup>/K<sup>+</sup>ATPase- $\alpha$ 3-swap-myc, followed by IB for SOD1, Na<sup>+</sup>/K<sup>+</sup>ATPase- $\alpha$ 3 and myc indicates loss of misfSOD1 association with Na<sup>+</sup>/K<sup>+</sup>ATPase- $\alpha$ 3-swap-myc

expression and the ratio of ionotropic receptor subunits thereby impacting neuronal transmission (Suppl. Fig. 2e). We examined whether altered Na<sup>+</sup>/K<sup>+</sup>ATPase- $\alpha$ 3 activity and altered expression of AMPA receptors lead to synaptic alterations onto MNs which has been previously shown [10, 49, 58, 59]. Na<sup>+</sup>/K<sup>+</sup>ATPase- $\alpha$ 3 was inhibited by administering Ouabain intraspinally in WT mice and spinal cords were analyzed 6 h, 12 h, 24 h or 3 days after Ouabain application. Immunostaining for VACht (marker for C-boutons; metabotropic cholinergic synapses which positively regulate MN excitability) revealed that acute Ouabain application increased the size of C-boutons onto WT MNs already after 6 h. By 24 h, a significant and stable increase in size





of C-boutons was observed. Additionally, in presymptomatic *G93A-s* mice, already enlarged C-boutons increased further in response to Ouabain (Fig. 4d). Besides being larger in volume, the average number of C-boutons contacting WT MN soma increased by a factor of two after 3 days of Ouabain treatment. In *G93A-s*, C-bouton numbers were slightly elevated and increased further to similar levels to that in WT Ouabain treated condition (Fig. 4d). These results indicate that not only suboptimal Na<sup>+</sup>/K<sup>+</sup>ATPase activity but the resulting alterations in GluR2 and GluR3 expression as well as synaptic inputs onto MNs might all synergistically modify MN excitability and influence the disease pathology.

### Early reduction in surface localized levels of Na<sup>+</sup>/K<sup>+</sup>ATPase- $\alpha$ 3 in the ventral horn

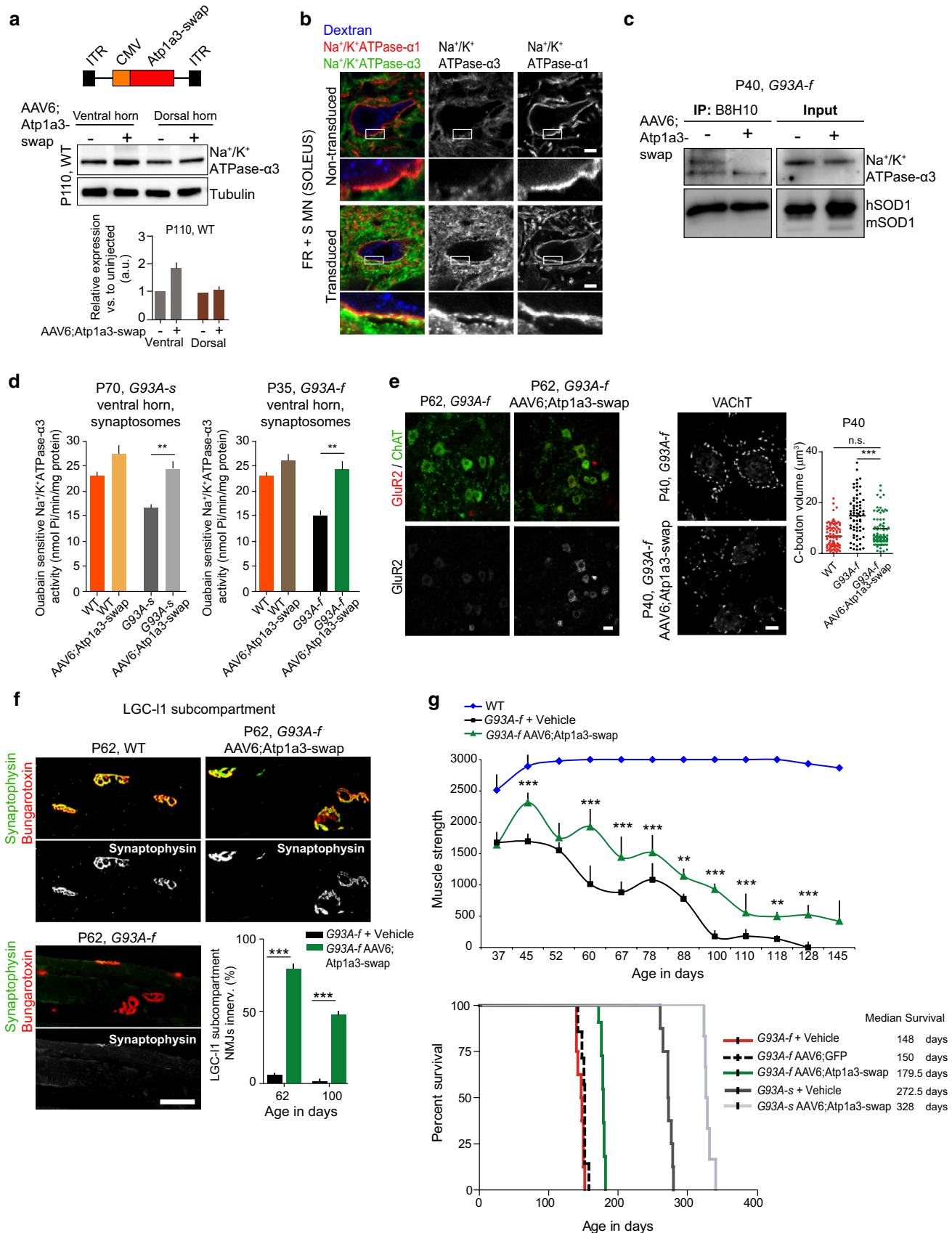
Since previous results suggested that misfSOD1 binds to Na<sup>+</sup>/K<sup>+</sup>ATPase-3 whose expression is enriched in FF MNs, and these MNs are most vulnerable in fALS, we examined the fate of Na<sup>+</sup>/K<sup>+</sup>ATPase- $\alpha$ 3 over disease course in *G93A-s* mice. As early as P25 in *G93A-s* mice, Na<sup>+</sup>/K<sup>+</sup>ATPase- $\alpha$ 3 colocalized with misfSOD1 in a fraction of B8H10 positive MNs. Between P75 and P100 this colocalization gradually increased and spread to approximately 55 % of lumbar MNs accounting for the known percentage of FF MNs in the lumbar region. Notably, with age, an increased intracellular staining for Na<sup>+</sup>/K<sup>+</sup>ATPase- $\alpha$ 3 was observed in *G93A-s* MNs (Fig. 5a). Surface biotinylation assays on spinal ventral horn slices from *G93A-s* and WT mice at different ages revealed that by P90, in *G93A-s* ventral horn, surface levels of Na<sup>+</sup>/K<sup>+</sup>ATPase- $\alpha$ 3 were decreased by 19.5 % compared to WT condition. Strikingly as from P125, *G93A-s* mice presented dramatic and persistent reduction (approximately 75 %) in surface levels of Na<sup>+</sup>/K<sup>+</sup>ATPase- $\alpha$ 3. Despite the reduction in membrane associated Na<sup>+</sup>/K<sup>+</sup>ATPase- $\alpha$ 3 as from P90, total protein levels remained unaltered until P125 and a reduction in total levels was only observed at a late age; P180 (Fig. 5b). This decline in surface associated Na<sup>+</sup>/K<sup>+</sup>ATPase- $\alpha$ 3 fraction was selective as this reduction was not observed for Na<sup>+</sup>/K<sup>+</sup>ATPase- $\alpha$ 1 at P125 (Suppl. Fig. 3a). At end stage of disease, surviving VACHT positive MNs which are predominantly S MNs exhibited negligible expression of Na<sup>+</sup>/K<sup>+</sup>ATPase- $\alpha$ 3. Moreover, neighboring VACHT negative neurons were free of misfSOD1 accumulation and presented membrane expression of Na<sup>+</sup>/K<sup>+</sup>ATPase- $\alpha$ 3 indicating that alterations in Na<sup>+</sup>/K<sup>+</sup>ATPase- $\alpha$ 3 levels were selective to MNs (Suppl. Fig. 3b).

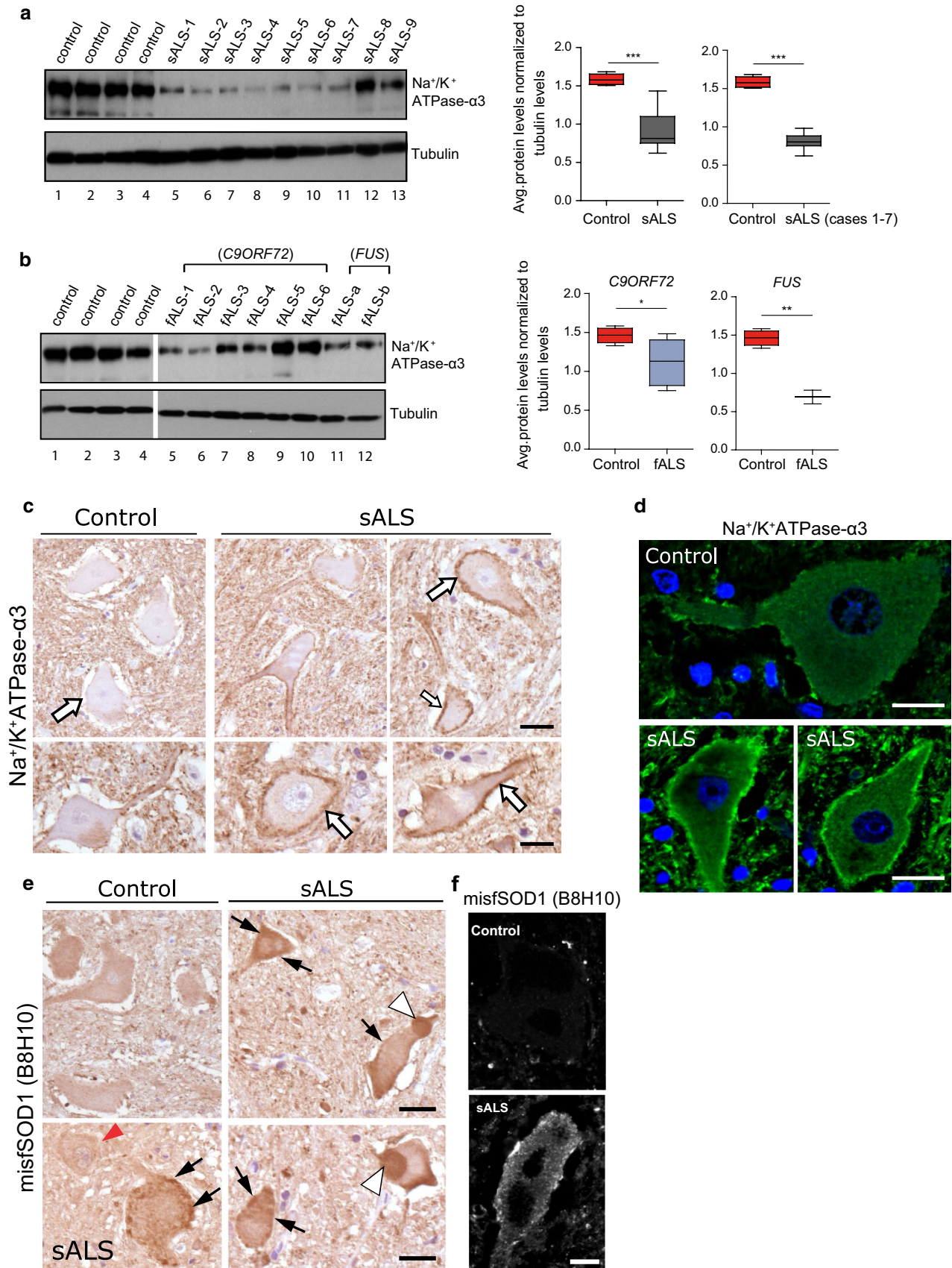
As Na<sup>+</sup>/K<sup>+</sup>ATPase- $\alpha$ 3 expression is lost from the surface followed by decline in expression at later ages, *G93A-s* spinal cord were transduced with lentivirus containing full length Na<sup>+</sup>/K<sup>+</sup>ATPase- $\alpha$ 3. Twenty five days post

**Fig. 7** Expression of misfSOD1 binding deficient Na<sup>+</sup>/K<sup>+</sup>ATPase- $\alpha$ 3 delays disease pathology. **a** Schematic depicting the generation of an AAV6 vector expressing full length cDNA of Na<sup>+</sup>/K<sup>+</sup>ATPase- $\alpha$ 3 containing the 10 amino acid swap (Atp1a3-swap). **Bottom** IB of spinal cord confirms increased expression of Na<sup>+</sup>/K<sup>+</sup>ATPase- $\alpha$ 3 in the ventral but not in the dorsal horn of AAV6;Atp1a3-swap injected P110, WT mice. Representative blot out of 2 experiments. **Q.A.** relative expression levels of Na<sup>+</sup>/K<sup>+</sup>ATPase- $\alpha$ 3 between injected and uninjected WT mice. **b** Confirmation of expression of Atp1a3-swap by dextran labeling of the Soleus motor pool in WT mice, revealing the expression of Na<sup>+</sup>/K<sup>+</sup>ATPase- $\alpha$ 3 in S MNs which endogenously do not express Na<sup>+</sup>/K<sup>+</sup>ATPase- $\alpha$ 3. **c** Reduced presence of misfSOD1-Na<sup>+</sup>/K<sup>+</sup>ATPase- $\alpha$ 3 complex in P40, *G93A-f* spinal cord transduced with AAV6;Atp1a3-swap compared to uninjected littermates. Co-IP performed using B8H10 antibody against misfSOD1 and IB for Na<sup>+</sup>/K<sup>+</sup>ATPase- $\alpha$ 3 and SOD1. **d** Measurement of Ouabain sensitive Na<sup>+</sup>/K<sup>+</sup>ATPase- $\alpha$ 3 activity in AAV6;Atp1a3-swap injected spinal ventral horn. The expression of AAV6;Atp1a3-swap leads to an increase in Na<sup>+</sup>/K<sup>+</sup>ATPase- $\alpha$ 3 activity in WT MNs and significantly rescues the observed Na<sup>+</sup>/K<sup>+</sup>ATPase- $\alpha$ 3 activity deficit in both *G93A-s* and *G93A-f* mice. Activity measurements are represented as the mean  $\pm$  SEM for all. \*\*\* $p$  < 0.0001,  $F_{(3,8)} = 14.79$  by ANOVA, \*\* $p$  = 0.0013 post-ANOVA Tukey's test for *G93A-s*. \*\*\* $p$  < 0.0001,  $F_{(3,8)} = 14.58$  by ANOVA, \*\* $p$  = 0.0013, for *G93A-f* mice by post-ANOVA Tukey's test,  $n = 3$  experiments with 4 mice/condition. **e** Immunolabeling for GluR2, sustained expression of the receptor in AAV6;Atp1a3-swap infected MNs at P62 in *G93A-f* mice. Labeling for C-boutons and measurements of their volumes in AAV6;Atp1a3-swap transduced P40, *G93A-f* MNs reveals comparable C-bouton volume as that in WT, indicated by the scatter plot (\*\*\* $p$  < 0.0001,  $F_{(2,252)} = 37.08$  by ANOVA, \*\*\* $p$  < 0.001 by post-ANOVA Tukey's test,  $n = 68$ –100 C-boutons from 3 mice/genotype). **f** Expression of misfSOD1 binding deficient Na<sup>+</sup>/K<sup>+</sup>ATPase- $\alpha$ 3 delays MN denervation. Analysis of the LGC-11 muscle subcompartment, purely innervated by FF MNs at P62 and at P100 in *G93A-f* mice exhibits preserved axonal innervation (presence of Synaptophysin labeling) compared to vehicle treated *G93A-f* mice. Note by P62 all *G93A-f* FF MNs have synchronously disconnected their target muscle fibers. Mean  $\pm$  SEM, unpaired  $t$  test, P62: \*\*\* $p$  < 0.0001,  $t(6) = 55.64$ , P100: \*\*\* $p$  < 0.0001,  $t(6) = 29.15$ ,  $n = 4$  mice/conditions. **g** AAV6;Atp1a3-swap expression ameliorates loss of muscle strength and extends life span of mutant mice. Values are the mean  $\pm$  SEM from 8 mice/genotype for muscle strength, two-way ANOVA, \*\*\* $p$  < 0.0001,  $F_{(2,22)} = 3820$  for genotype and \*\* $p$  < 0.01, \*\*\* $p$  < 0.001 by Bonferroni test between *G93A-f* + Vehicle and *G93A-f* AAV6;Atp1a3-swap. Survival: cumulative survival of *G93A-f*, *G93A-s* mice infected with AAV6;Atp1a3-swap and *G93A-f* infected with AAV6;GFP,  $n = G93A-f$  + Vehicle = 8, *G93A-f* AAV6;Atp1a3-swap = 12, *G93A-f* + GFP = 7 mice, *G93A-s* + Vehicle = 8, *G93A-s* AAV6;Atp1a3-swap = 6 mice. Median survival values are indicated next to the figure. Log rank (Mantel Cox test) = 48.84, \*\*\* $p$  < 0.0001. Scale **b** 10, **e** 10, 20, **f** 20  $\mu$ m

infection, measurements of the Na<sup>+</sup>/K<sup>+</sup>ATPase- $\alpha$ 3 activity from the ventral horn revealed an improvement of only 10 % in activity. However, this improvement in activity did not protect NMJs which were denervated at comparable times to those of non-transduced littermates. Further, exogenous expression of Na<sup>+</sup>/K<sup>+</sup>ATPase- $\alpha$ 3 did not prolong the life span of mutant mice, suggesting that compensating the Na<sup>+</sup>/K<sup>+</sup>ATPase- $\alpha$ 3 expression in mutSOD1







◀ **Fig. 8** ALS spinal cords present B8H10 positive misfSOD1 and altered Na<sup>+</sup>/K<sup>+</sup>ATPase-α3 expression. **a** Na<sup>+</sup>/K<sup>+</sup>ATPase-α3 is downregulated in spinal cord of sporadic ALS (sALS) patients. **IB** from control cases (*n* = 4) and patients with sALS (*n* = 9) displays reduced protein levels of Na<sup>+</sup>/K<sup>+</sup>ATPase-α3. **Right** Q.A. of average protein levels normalized to internal loading control tubulin, \*\*\**p* = 0.0004, unpaired *t* test, *t*(11) = 4.990. **Extreme right** patient cases (sALS1–7) show negligible amounts of Na<sup>+</sup>/K<sup>+</sup>ATPase-α3, observed by the relative Na<sup>+</sup>/K<sup>+</sup>ATPase-α3 levels, \*\*\**p* < 0.0001, unpaired *t* test, *t*(9) = 12.05. Representative blot from 4 experiments. **b** **IB** from control cases (*n* = 4) and patients with familial ALS (fALS) harboring mutations in the *C9ORF72* gene (*n* = 6) or *FUS* gene (*n* = 2) show reduced Na<sup>+</sup>/K<sup>+</sup>ATPase-α3 levels. **Right** Q.A. of average Na<sup>+</sup>/K<sup>+</sup>ATPase-α3 levels normalized to internal loading control tubulin, \**p* = 0.0486, unpaired *t* test, *t*(8) = 2.324. Of the 6 samples, fALS cases 1–4 show stronger reduction in Na<sup>+</sup>/K<sup>+</sup>ATPase-α3 expression compared to cases fALS-5 and fALS-6 which have near normal expression. **Extreme right** Q.A. of average Na<sup>+</sup>/K<sup>+</sup>ATPase-α3 levels normalized to internal loading control tubulin for fALS cases with *FUS* mutations, \*\**p* = 0.017, unpaired *t* test, *t*(4) = 7.546. **c** Immunohistochemical staining for Na<sup>+</sup>/K<sup>+</sup>ATPase-α3 in spinal cord tissues from humans with sALS as compared to unaffected controls. Note the increased plasma membrane-associated labeling for Na<sup>+</sup>/K<sup>+</sup>ATPase-α3 in some of the surviving sALS MNs. For a lower power comparative view, see Suppl. Fig. 8a. **d** Immunofluorescence staining of sALS and control alpha-MNs showing broader surface localization of Na<sup>+</sup>/K<sup>+</sup>ATPase-α3 in two of the remaining sALS MNs as compared to the control, where a fine outline of Na<sup>+</sup>/K<sup>+</sup>ATPase-α3 around the MN soma is observed. **e** Presence of B8H10 immunopositive misfSOD1 in human sALS patient spinal cord. Immunohistochemical misfSOD1 staining on MNs in humans with sALS as compared to unaffected controls; **black arrows** mark staining for misfSOD1 associated with the plasma membrane of MNs. Large intracellular aggregate reactive with the B8H10 antibody are indicated by **arrow heads**. **Red arrow head** marks an adjacent MN negative for misfSOD1 immunoreactivity. **f** Immunofluorescence staining of sALS and control alpha-MNs incubated with B8H10 antibody displaying subplasmalemmal accumulation of misfSOD1 in the sALS MN. **Scale bar** **c** 25, **d** 40, **e** 30, **f** 20 μm

background was not sufficient to rescue the pathology (Suppl. Fig. 4a–c).

We next examined the discrepancy between the early reduced surface and unchanged total levels of Na<sup>+</sup>/K<sup>+</sup>ATPase-α3. Immunostainings of spinal cord sections revealed an increased immunoreactivity for Na<sup>+</sup>/K<sup>+</sup>ATPase-α3 in the ER together with ER chaperone BiP in MNs of *G93A-s* and *G93A-f*, but not in WT and *tg-wt* MNs (Fig. 5c). Microsomal fractions enriched in ER membranes from ventral horn of *G93A-s* and WT mice revealed that in *G93A-s* at P125, prominent accumulation of Na<sup>+</sup>/K<sup>+</sup>ATPase-α3 within ER membrane fractions occurs (Fig. 5d). Note that ER associated mutSOD1 levels did not change from P90 to P125. As FF MNs already exhibit UPR at P125, we monitored whether relieving ER stress would restore Na<sup>+</sup>/K<sup>+</sup>ATPase-α3 activity. Delivery of ER stress alleviator Salubrinal to *G93A-s* mice led to the re-localization of Na<sup>+</sup>/K<sup>+</sup>ATPase-α3 to the MN surface (Fig. 5e), which led to a partial recovery in Na<sup>+</sup>/K<sup>+</sup>ATPase-α3 activity (approximately 50 %) in *G93A-s* compared to untreated

mice (Fig. 5f). We examined whether ER stress could drive ER accumulation of surface associated Na<sup>+</sup>/K<sup>+</sup>ATPase-α3. Early delivery of ER stress inducer Tunicamycin to *G93A-s* mice at P49 (55–60 days before UPR in FF MNs) followed by measurement of Na<sup>+</sup>/K<sup>+</sup>ATPase-α3 activity revealed no decline in activity compared to the untreated *G93A-s* mice (Suppl. Fig. 5a). Moreover, high ER stress at this early time point did not lead to the mislocalization of surface bound Na<sup>+</sup>/K<sup>+</sup>ATPase-α3 to the ER (Suppl. Fig. 5b), hinting towards a probable ER retention of newly synthesized Na<sup>+</sup>/K<sup>+</sup>ATPase-α3 at a specific stage in disease coinciding with UPR.

#### Direct association of misfSOD1 with Na<sup>+</sup>/K<sup>+</sup>ATPase-α3 via residues 484–493 in the nucleotide binding domain of Na<sup>+</sup>/K<sup>+</sup>ATPase-α3

As Na<sup>+</sup>/K<sup>+</sup>ATPase-α3 is a transmembrane pump with a large cytoplasmic nucleotide-binding domain (N), encompassing residues 372–586 (Fig. 6a), we hypothesized that the aberrant interaction between the protein and misfSOD1 occurs via the intracellular N-domain. Consistent with our hypothesis, the expression of C-terminal myc-tagged nucleotide binding domain (N-myc) of Na<sup>+</sup>/K<sup>+</sup>ATPase-α3 together with hSOD1G93A or WT-hSOD1 in mouse neuroblastoma (n2a) cells revealed a selective association of B8H10 positive misfSOD1 but not of WT-hSOD1 with N-myc. To further clarify that WT-hSOD1 did not associate with N-myc, a reverse co-IP with myc antibody was performed which revealed no association between the two (Fig. 6b). Various SOD1 mutants interacted with the same N-domain of Na<sup>+</sup>/K<sup>+</sup>ATPase-α3 (Fig. 6c), hinting towards a conserved conformational state of misfSOD1 which determined this interaction. Notably, this association was lost when hSOD1G93A and Na<sup>+</sup>/K<sup>+</sup>ATPase-α3 lacking the N-domain (residues 375–583 deleted and termed as ΔN-myc) were co-expressed together (Fig. 6d). To gain insights into the interaction, purified recombinant N-terminal His-tagged N-domain of Na<sup>+</sup>/K<sup>+</sup>ATPase-α3 (His-N), WT-hSOD1 or hSOD1G93A proteins were incubated together. **IB** for His-N and hSOD1 revealed that hSOD1G93A directly interacts with the N-domain of Na<sup>+</sup>/K<sup>+</sup>ATPase-α3 (Fig. 6e). Note that we used n2a cells as they do not show endogenous Na<sup>+</sup>/K<sup>+</sup>ATPase-α3 expression. Transient expression of hSOD1G93A but not WT-hSOD1 with Na<sup>+</sup>/K<sup>+</sup>ATPase-α3 in n2a cells leads to their co-accumulation into aggregate like structures (Suppl. Fig. 6a, b).

Having established a direct interaction between misfSOD1 and Na<sup>+</sup>/K<sup>+</sup>ATPase-α3 via its N-domain, we aimed to further narrow down the site of this interaction. Aligning the N-domains of homologous Na<sup>+</sup>/K<sup>+</sup>ATPase-α3 and Na<sup>+</sup>/K<sup>+</sup>ATPase-α1 revealed 78 % sequence identity and highlighted distinct stretches of residues which are



different thereby likely determining specificity of the interaction (Fig. 6f). Homology modeling of the N-domain of mouse Na<sup>+</sup>/K<sup>+</sup>ATPase- $\alpha$ 3 using the crystal structure of the *S. acanthias* Na<sup>+</sup>/K<sup>+</sup>ATPase as template [60] (PDB 2ZXE, 77 % sequence identity in the N-domain) enabled us to map these differences onto the N-domain surface for a structure function analysis (Fig. 6g). Strikingly, all residue changes between the N-domains of Na<sup>+</sup>/K<sup>+</sup>ATPase- $\alpha$ 3 and Na<sup>+</sup>/K<sup>+</sup>ATPase- $\alpha$ 1 reside on the surface opposite of the nucleotide-binding cleft whereas the domain surface that binds ATP and interacts with the actuator (A) and the phosphorylation (P) cytosolic domains of the Na<sup>+</sup>/K<sup>+</sup>ATPase- $\alpha$ 3 chain are completely conserved. Additionally, the longest continuous N-domain sequence stretch that differs between Na<sup>+</sup>/K<sup>+</sup>ATPase- $\alpha$ 3 and Na<sup>+</sup>/K<sup>+</sup>ATPase- $\alpha$ 1, residues 484–493, forms a distinct solvent exposed acidic loop thereby providing a putative interaction site for misfSOD1. To test this hypothesis, n2a cells were transfected either with hSOD1G93A or WT-hSOD1 and a myc-tagged Na<sup>+</sup>/K<sup>+</sup>ATPase- $\alpha$ 3 construct where residues 484–493 were exchanged to the corresponding residues of Na<sup>+</sup>/K<sup>+</sup>ATPase- $\alpha$ 1 termed as Na<sup>+</sup>/K<sup>+</sup>ATPase- $\alpha$ 3-swap-myc, followed by co-IP with SOD1. The binding of hSOD1G93A to Na<sup>+</sup>/K<sup>+</sup>ATPase- $\alpha$ 3-swap-myc was lost (Fig. 6h), indicating that the acidic loop in Na<sup>+</sup>/K<sup>+</sup>ATPase- $\alpha$ 3 is the probable site for association with misfSOD1.

#### Expression of misfSOD1 binding deficient Na<sup>+</sup>/K<sup>+</sup>ATPase- $\alpha$ 3 restores Na<sup>+</sup>/K<sup>+</sup>ATPase-activity and prolongs survival of mutant SOD1G93A mice

Next, to determine whether the binding of misfSOD1 to Na<sup>+</sup>/K<sup>+</sup>ATPase- $\alpha$ 3 leading to the impairment in its ATPase activity also influences the disease pathophysiology, misfSOD1 binding deficient Na<sup>+</sup>/K<sup>+</sup>ATPase- $\alpha$ 3 where residues 484–493 were replaced by corresponding residues from Na<sup>+</sup>/K<sup>+</sup>ATPase- $\alpha$ 1 (494–503), was expressed in MNs via adeno-associated virus (AAV6), referred to as AAV6;Atp1a3-swap. This chimeric Na<sup>+</sup>/K<sup>+</sup>ATPase- $\alpha$ 3 pump was fully functional as assessed by the measurement of its ATPase activity in n2a cells (Suppl. Fig. 7). IB for Na<sup>+</sup>/K<sup>+</sup>ATPase- $\alpha$ 3 after transduction of spinal cord with AAV6;Atp1a3-swap revealed a two-fold increase in the expression of Na<sup>+</sup>/K<sup>+</sup>ATPase- $\alpha$ 3 in WT ventral horn spinal cord (Fig. 7a). As further evidence, MNs from the soleus muscle were labeled with RITC-dextran. Approximately 85 % of soleus MNs presented expression of Na<sup>+</sup>/K<sup>+</sup>ATPase- $\alpha$ 3 compared to non-transduced soleus MNs, where 50 % of soleus MNs express negligible amounts of Na<sup>+</sup>/K<sup>+</sup>ATPase- $\alpha$ 3 (Fig. 7b). Co-IP of misfSOD1 from P40, *G93A-f* spinal cord via B8H10 antibody revealed a decline in misfSOD1-Na<sup>+</sup>/K<sup>+</sup>ATPase- $\alpha$ 3 complex in

AAV6;Atp1a3-swap transduced *G93A-f* spinal cords (Fig. 7c). Subsequent measurements of Na<sup>+</sup>/K<sup>+</sup>ATPase- $\alpha$ 3 activity revealed prominent rescue of Na<sup>+</sup>/K<sup>+</sup>ATPase- $\alpha$ 3 activity in both mouse models. Notably, the restoration of Na<sup>+</sup>/K<sup>+</sup>ATPase- $\alpha$ 3 activity in P35, *G93A-f* and P70, *G93A-s* MNs was to a similar extent as in WT conditions (Fig. 7d). The rescue in Na<sup>+</sup>/K<sup>+</sup>ATPase- $\alpha$ 3 activity led to a high and sustained GluR2 expression levels in AAV6;Atp1a3-swap infected P62, *G93A-f* MNs compared to uninfected littermates. C-bouton in SOD1G93A mice which were transduced with AAV6;Atp1a3-swap were smaller than those on non-transduced MNs and near similar in volume to those in WT conditions (Fig. 7e). Further, NMJs exhibited sustained axonal innervation and 80 % of disease vulnerable FF MN innervated endplates were preserved at P62 (Fig. 7f). At a behavioral level, *G93A-f* AAV6;Atp1a3-swap injected mice presented improved muscle strength as measured by the grid test (Fig. 7g). Despite the presence of mutSOD1 protein and endogenous Na<sup>+</sup>/K<sup>+</sup>ATPase- $\alpha$ 3, the expression of AAV6;Atp1a3-swap prolonged the life span of *G93A-f* and *G93A-s* mice (Fig. 7h).

#### Altered Na<sup>+</sup>/K<sup>+</sup>ATPase- $\alpha$ 3 expression in fALS and sALS patients

Lastly, we examined whether alterations in Na<sup>+</sup>/K<sup>+</sup>ATPase- $\alpha$ 3 expression levels would also be present in non-SOD1 mediated fALS and sALS as alterations in MN excitability has been observed in both forms of ALS in humans, as well as in iPSC cells from patients differentiated into MNs [13, 66–68]. Examining lumbar human spinal cord tissue for Na<sup>+</sup>/K<sup>+</sup>ATPase- $\alpha$ 3 expression from control and sALS patients revealed that in four age matched cases, strong expression of Na<sup>+</sup>/K<sup>+</sup>ATPase- $\alpha$ 3 was observed. In contrast, of the nine cases of sALS patients examined, seven cases (sALS-1–7, lanes 5–11) revealed a strong reduction in Na<sup>+</sup>/K<sup>+</sup>ATPase- $\alpha$ 3 levels (Fig. 8a). One sALS case (sALS-8, lane 12) presented near normal expression of Na<sup>+</sup>/K<sup>+</sup>ATPase- $\alpha$ 3 when compared to control cases. Further, alterations in the expression of Na<sup>+</sup>/K<sup>+</sup>ATPase- $\alpha$ 3 was observed in non-SOD1 mediated fALS cases. Of the six cases related to mutations in the *C9ORF72* gene; four cases (fALS-1–4, lanes 5–8) presented lower levels of Na<sup>+</sup>/K<sup>+</sup>ATPase- $\alpha$ 3 while the other two cases (fALS-5–6) presented Na<sup>+</sup>/K<sup>+</sup>ATPase- $\alpha$ 3 expression similar to control cases (Fig. 8b). Both cases harboring mutations in the *FUS* gene exhibited reduced Na<sup>+</sup>/K<sup>+</sup>ATPase- $\alpha$ 3 expression (Fig. 8b). Immunohistochemical analysis revealed that in the control group as expected, basal Na<sup>+</sup>/K<sup>+</sup>ATPase- $\alpha$ 3 immunoreactivity finely outlined the periphery of the MN soma. Interestingly, some of the surviving MNs (10–20 %) from human sALS spinal cord showed increased Na<sup>+</sup>/K<sup>+</sup>ATPase- $\alpha$ 3; in several representative examples broad



ruffled plasma membrane-associated Na<sup>+</sup>/K<sup>+</sup>ATPase- $\alpha$ 3 staining was observed (Fig. 8c–d; Suppl. Fig. 8). Further, immunostaining for misfSOD1 revealed that several sALS cases presented immunolabeling for misfSOD1. misfSOD1 immunoreactivity was not restricted to large globular intracellular aggregates (arrow heads), but was also found close to the plasma membrane in the form of diffuse or slightly speckled staining (black arrows) (Fig. 8e–f) similar to the labeling observed for Na<sup>+</sup>/K<sup>+</sup>ATPase- $\alpha$ 3.

## Discussion

Our work provides a mechanistic explanation for how expression of mutSOD1 might contribute to altering MN excitability in fALS. Profiting from the B8H10 antibody which detects a disease specific epitope on misfSOD1 in vulnerable FF MNs as from P7 in *G93A-s* mice, we performed a longitudinal unbiased proteomic screen of the misfolded SOD1G93A interactome. This provided the earliest signature of proteins interacting with misfSOD1 and led to the identification of a core group of aberrant interactions which included Na<sup>+</sup>/K<sup>+</sup>ATPase- $\alpha$ 3. The early and consistent interaction of misfSOD1 with the N-domain of Na<sup>+</sup>/K<sup>+</sup>ATPase- $\alpha$ 3 led to functional impairment of its ATPase activity in MN associated regions of the spinal cord. This impairment of Na<sup>+</sup>/K<sup>+</sup>ATPase- $\alpha$ 3 activity further modified GluR2 expression levels and cholinergic C-bouton inputs onto MNs. Notably, Na<sup>+</sup>/K<sup>+</sup>ATPase- $\alpha$ 3 expression was enriched within disease vulnerable FF MNs whereas its expression was the lowest in disease resistant MNs. AAV mediated expression of misfSOD1 binding deficient Na<sup>+</sup>/K<sup>+</sup>ATPase- $\alpha$ 3 in vivo restored Na<sup>+</sup>/K<sup>+</sup>ATPase- $\alpha$ 3 activity in spinal cord, delayed pathological alterations associated with MN excitability and prolonged significantly the life span of mutSOD1 mice.

Na<sup>+</sup>/K<sup>+</sup>ATPase- $\alpha$ 3 is an integral neuronal membrane protein exporting three Na<sup>+</sup> ions and importing two K<sup>+</sup> ions for each ATP hydrolyzed and is a major determinant of neuronal resting membrane potential [15]. Therefore, suboptimal functioning of the ATP-driven ion pump will lead to elevated intracellular Na<sup>+</sup> levels resulting in a higher resting potential which at first might account for hyperexcitability and eventually lead to the collapse of membrane potential. Furthermore, the tight functional coupling between glutamate receptors and Na<sup>+</sup>/K<sup>+</sup>ATPase is required for the maintenance of intraspinal synaptic function. The suppression or diminishing of Na<sup>+</sup>/K<sup>+</sup>ATPase activity causes the rapid internalization and proteasome-mediated degradation of AMPA receptors (AMPA), resulting in lasting suppression of AMPAR-mediated synaptic transmission [70]. An early and a prominent reduction in GluR2 has been found in presymptomatic *G93A-f* mice

[61], and our work has revealed that impaired or diminished Na<sup>+</sup>/K<sup>+</sup>ATPase- $\alpha$ 3 activity influences this reduction, which could be rescued by the viral mediated expression of misfSOD1 binding deficient Na<sup>+</sup>/K<sup>+</sup>ATPase- $\alpha$ 3. These results indicate that sub-optimal Na<sup>+</sup>/K<sup>+</sup>ATPase- $\alpha$ 3 functioning might not only alter membrane potential but concomitantly influence neuronal transmission in the spinal cord.

Impairment in Na<sup>+</sup>/K<sup>+</sup>ATPases can be recapitulated in other neurodegenerative diseases, where selective neuronal vulnerabilities due to altered excitability predispose them to degeneration [57]. DJ-1 mutations causing early onset Parkinson's disease (PD) confer neuronal vulnerability via energy metabolism deficits leading to impairments in Na<sup>+</sup>/K<sup>+</sup>ATPase activity to which mutant substantia nigra pars compacta neurons (SNpc) are particularly sensitive [48]. SNpc neurons mainly express Na<sup>+</sup>/K<sup>+</sup>ATPase- $\alpha$ 3 and are vulnerable to mutations in the Na<sup>+</sup>/K<sup>+</sup>ATPase- $\alpha$ 3 gene, leading to Rapid Onset Dystonia Parkinson [12]. In Alzheimer's disease (AD), the activity of Na<sup>+</sup>/K<sup>+</sup>ATPase is significantly lower in the brains of patients with AD than in the brains of normal controls and directly correlates with impaired neuronal function [36]. Interestingly, the exposure of synaptosomes isolated from postmortem human hippocampus to A $\beta$  selectively reduced Na<sup>+</sup>/K<sup>+</sup>ATPase and Ca<sup>2+</sup>ATPase activities, but not the activities of Mg<sup>2+</sup>-dependent ATPase or Na<sup>+</sup>/Ca<sup>2+</sup> exchanger, suggesting that impairments in ATPase activities associated with ion movements might correlate with the pathogenesis of AD [41]. In fALS, a progressive loss of expression of all three Na<sup>+</sup>/K<sup>+</sup>ATPases at end stage in *G93A-f* mice has been shown [16]. Moreover, this study also examined other factors such as increased nitric oxide which could contribute to the reduction in Na<sup>+</sup>/K<sup>+</sup>ATPase activity and found that high basal levels of nitric oxide was not causally associated with the observed impairment in *G93A-f* mice [16]. In this context, our finding of a selective association of misfSOD1 with Na<sup>+</sup>/K<sup>+</sup>ATPase- $\alpha$ 3 and the resultant impairment in its ATPase activity provides incremental insights into how early impairments in Na<sup>+</sup>/K<sup>+</sup>ATPase- $\alpha$ 3 activity could selectively alter MN excitability in mutSOD1 mediated fALS.

Na<sup>+</sup>/K<sup>+</sup>ATPase- $\alpha$ 1 is ubiquitously expressed, whereas Na<sup>+</sup>/K<sup>+</sup>ATPase- $\alpha$ 3 exhibits a restricted neuronal expression pattern, and both proteins can occur together or singly in neurons [30, 42] which is probably indicative of their specialized functions. We show that FF MNs predominantly express Na<sup>+</sup>/K<sup>+</sup>ATPase- $\alpha$ 3, whereas S MNs mainly express Na<sup>+</sup>/K<sup>+</sup>ATPase- $\alpha$ 1 and that B8H10 immunoreactive misfSOD1 specifically binds to Na<sup>+</sup>/K<sup>+</sup>ATPase- $\alpha$ 3. This suggests that early impairment in Na<sup>+</sup>/K<sup>+</sup>ATPase- $\alpha$ 3 function might initially and rather selectively impact FF MNs. Functional differences between Na<sup>+</sup>/K<sup>+</sup>ATPase

isozymes are observed with regards to their affinity for  $\text{Na}^+$ , where  $\text{Na}^+/\text{K}^+\text{ATPase-}\alpha 3$  has lower affinity for  $\text{Na}^+$  than  $\text{Na}^+/\text{K}^+\text{ATPase-}\alpha 1$  [44].  $\text{Na}^+/\text{K}^+\text{ATPase-}\alpha 1$  plays a major role in maintaining basal intracellular  $\text{Na}^+$  levels, whereas  $\text{Na}^+/\text{K}^+\text{ATPase-}\alpha 3$  plays an important role in controlling resting membrane potential. Particularly, the function of  $\text{Na}^+/\text{K}^+\text{ATPase-}\alpha 3$  is crucial during suprathreshold neuronal activity that leads to rapid large intracellular increase in  $\text{Na}^+$  levels [4]. Moreover, the recovery of intracellular  $\text{Na}^+$  levels after suprathreshold activity requires increased  $\text{Na}^+/\text{K}^+\text{ATPase-}\alpha 3$  activity and subsequently greater energy consumption. In general,  $\text{Na}^+/\text{K}^+\text{ATPase}$  pump activity uses approximately 50 % of ATP generated by the neurons and it is of interest to note that  $\text{Na}^+/\text{K}^+\text{ATPase-}\alpha 3$  exhibits higher ATP-affinity compared to  $\alpha 1$  [7]. Computational modeling of selective MN vulnerability in ALS suggested that deficits in ATP production and consumption might directly impair  $\text{Na}^+/\text{K}^+\text{ATPase}$  homeostasis thereby generating a deadly feedback loop. Such a deficit would be catastrophic to neurons, causing incomplete repolarization and making them more inclined to fire, eventually leading to complete loss of firing when the membrane potential becomes too depolarized [34]. Since muscle contractions induced by FF MNs are powerful but short lived and the recruitment of FF MNs requires crossing a high excitability threshold, the finding that FF MNs mainly express  $\text{Na}^+/\text{K}^+\text{ATPase-}\alpha 3$  might corroborate well with the proposed function of  $\text{Na}^+/\text{K}^+\text{ATPase-}\alpha 3$ . However, at the same time, the high demand for ATP to maintain optimal  $\text{Na}^+/\text{K}^+\text{ATPase-}\alpha 3$  functioning might expose FF MNs to vulnerability in conditions associated with suboptimal functioning of  $\text{Na}^+/\text{K}^+\text{ATPase-}\alpha 3$  and ATP generation.

We show that misfSOD1 interacts with the cytosolic N-domain of  $\text{Na}^+/\text{K}^+\text{ATPase-}\alpha 3$  and have mapped this interaction to an isoform-specific solvent exposed acidic loop (residues 484–493) opposite of the nucleotide binding site. This leads to reduced ATPase activity (measured as free Pi levels produced by  $\text{Na}^+/\text{K}^+\text{ATPase-}\alpha 3$ ) already at P50 when the surface levels of the pump are still the same for WT and *G93A-s* (Figs. 2b, 5b). With this we can speculate about how misfSOD1 might impair the function of the  $\text{Na}^+/\text{K}^+$  pump: as the ATP binding site on the N-domain is located opposite of the acidic loop where misfSOD1 interacts, the aberrant association likely allows ATP binding but might prevent autophosphorylation or any subsequent conformational change needed for  $\text{Na}^+$  release to the extracellular space or  $\text{K}^+$  uptake from the cytosol. This suggests that  $\text{Na}^+/\text{K}^+\text{ATPase-}\alpha 3$  is blocked anywhere between  $\text{Na}_3\text{E1ATP}$  and  $\text{K}_2\text{E2-P}$  state leading to perturbed cellular ion concentrations and membrane resting potential. The initial and early decline by 22 % in  $\text{Na}^+/\text{K}^+\text{ATPase-}\alpha 3$  activity measured at P50 would then be sufficient to overload the remaining normally functioning  $\text{Na}^+/\text{K}^+\text{ATPase-}\alpha 3$ .

This, together with reduced ATP availability due to defective mitochondrial functioning as suggested by Le Masson et al. [34], might launch a vicious cycle accentuating  $\text{Na}^+/\text{K}^+\text{ATPase}$  deficits in disease.

We further show that  $\text{Na}^+/\text{K}^+\text{ATPase-}\alpha 3$  levels were altered in ALS patient tissues, suggesting that alterations in  $\text{Na}^+/\text{K}^+\text{ATPase-}\alpha 3$  levels are pathogenesis related. Since both aging and oxidative stress impair  $\text{Na}^+/\text{K}^+\text{ATPase}$  activity [20, 33], it is plausible that these factors could actively impair  $\text{Na}^+/\text{K}^+\text{ATPase-}\alpha 3$  function which then might serve as an important determinant for MN dysfunction in sALS and fALS. Another possibility for altered  $\text{Na}^+/\text{K}^+\text{ATPase-}\alpha 3$  levels could be related to the observation that WT-SOD1 in sALS cases undergoes age and environment associated modifications, causing conformational alterations in the structure of WT-SOD1, leading to a gain of toxic properties similar to those in mutSOD1 [9, 18, 25]. Here, one could imagine the toxic conformation alterations in WT-SOD1 might enable it to aberrantly associate with  $\text{Na}^+/\text{K}^+\text{ATPase-}\alpha 3$ , impairing its function and providing a link between altered MN excitability and ALS pathogenesis. Regarding the reasons for the apparent discrepancy between the  $\text{Na}^+/\text{K}^+\text{ATPase-}\alpha 3$  immunoblot and immunohistochemistry data, we think that the reduction in  $\text{Na}^+/\text{K}^+\text{ATPase-}\alpha 3$  protein levels in the immunoblots is due to the overall reduction in  $\alpha$ -MN numbers and also due to the fact that only 10–20 % of the remaining  $\alpha$ -MNs showed the increased plasma membrane-associated  $\text{Na}^+/\text{K}^+\text{ATPase-}\alpha 3$  labeling. In conclusion, our results provide experimental and mechanistic insights into the relationships between misfSOD1 accumulation and alterations in MN excitability and spinal connectivity in fALS. We identify impairment in  $\text{Na}^+/\text{K}^+\text{ATPase-}\alpha 3$  activity as being a determinant for selective vulnerability of MNs in disease and provide valuable new avenues for potential therapeutic strategies.

**Acknowledgments** This work was supported by Swiss National Science Foundation Professorship grants (PP00P3\_128460, PP00P3\_150756) and Frick foundation for ALS research to S.S., C.R., N.M. and A.FdLE. A.G. and J.W. were supported by a START program grant, Medical Faculty, RWTH Aachen University, by the Interdisciplinary Center for Clinical Research, IZKF Aachen (N5–3), and by the German Research Foundation, DFG (WE 1406/13–1).

#### Compliance with ethical standards

**Conflict of interest** The authors declare that no conflict of interests exists.

#### References

1. Al Kaabi A, Traupe T, Stutz M, Buchs N, Heller M (2012) Cause or effect of arteriogenesis: compositional alterations of micro-particles from CAD patients undergoing external counterpulsation therapy. PLoS One 7:e46822

2. Andersen PM, Nilsson P, Ala-Hurula V, Keranen ML, Tarvainen I, Haltia T, Nilsson L, Binzer M, Forsgren L, Marklund SL (1995) Amyotrophic lateral sclerosis associated with homozygosity for an Asp90Ala mutation in CuZn-superoxide dismutase. *Nat Genet* 10:61–66
3. Atkin JD, Farg MA, Walker AK, McLean C, Tomas D, Horne MK (2008) Endoplasmic reticulum stress and induction of the unfolded protein response in human sporadic amyotrophic lateral sclerosis. *Neurobiol Dis* 30:400–407
4. Azarias G, Kruusmagi M, Connor S, Akkuratov EE, Liu XL, Lyons D, Brismar H, Broberger C, Aperia A (2013) A specific and essential role for Na, K-ATPase alpha3 in neurons co-expressing alpha1 and alpha3. *J Biol Chem* 288:2734–2743
5. Bergh J, Zetterstrom P, Andersen PM, Brannstrom T, Graffmo KS, Jonsson PA, Lang L, Danielsson J, Oliveberg M, Marklund SL (2015) Structural and kinetic analysis of protein-aggregate strains in vivo using binary epitope mapping. *Proc Natl Acad Sci USA* 112:4489–4494. doi:10.1073/pnas.1419228112
6. Berrow NS, Alderton D, Owens RJ (2009) The precise engineering of expression vectors using high-throughput In-Fusion PCR cloning. *Methods Mol Biol* 498:75–90. doi:10.1007/978-1-59745-196-3\_5
7. Blanco G, Sanchez G, Mercer RW (1995) Comparison of the enzymatic properties of the Na, K-ATPase alpha 3 beta 1 and alpha 3 beta 2 isozymes. *Biochemistry* 34:9897–9903
8. Bories C, Amendola J, Lamotte d'Incamps B, Durand J (2007) Early electrophysiological abnormalities in lumbar motoneurons in a transgenic mouse model of amyotrophic lateral sclerosis. *Eur J Neurosci* 25:451–459
9. Bosco DA, Morfini G, Karabacak NM, Song Y, Gros-Louis F, Pasinelli P, Goolsby H, Fontaine BA, Lemay N, McKenna-Yasek D, Frosch MP, Agar JN, Julien JP, Brady ST, Brown RH Jr (2010) Wild-type and mutant SOD1 share an aberrant conformation and a common pathogenic pathway in ALS. *Nat Neurosci* 13:1396–1403. doi:10.1038/nn.2660
10. Chang Q, Martin LJ (2009) Glycinergic innervation of motoneurons is deficient in amyotrophic lateral sclerosis mice: a quantitative confocal analysis. *Am J Pathol* 174:574–585. doi:10.2353/ajpath.2009.080557
11. Costes SV, Daelemans D, Cho EH, Dobbin Z, Pavlakis G, Lockett S (2004) Automatic and quantitative measurement of protein-protein colocalization in live cells. *Biophys J* 86:3993–4003
12. de Carvalho Aguiar P, Sweadner KJ, Penniston JT, Zaremba J, Liu L, Caton M, Linazasoro G, Borg M, Tijssen MA, Bressman SB, Dobyns WB, Brashear A, Ozelius LJ (2004) Mutations in the Na<sup>+</sup>/K<sup>+</sup>-ATPase alpha3 gene ATP1A3 are associated with rapid-onset dystonia parkinsonism. *Neuron* 43:169–175
13. Devlin AC, Burr K, Borooah S, Foster JD, Cleary EM, Geti I, Vallier L, Shaw CE, Chandran S, Miles GB (2015) Human iPSC-derived motoneurons harbouring TARDBP or C9ORF72 ALS mutations are dysfunctional despite maintaining viability. *Nat Commun* 6:5999. doi:10.1038/ncomms6999
14. Dirren E, Towne CL, Setola V, Redmond DE Jr., Schneider BL, Aebischer P (2014) Intracerebroventricular injection of adeno-associated virus 6 and 9 vectors for cell type-specific transgene expression in the spinal cord. *Hum Gene Ther* 25:109–120
15. Dobretsov M, Stimers JR (2005) Neuronal function and alpha3 isoform of the Na/K-ATPase. *Front Biosci* 10:2373–2396
16. Ellis DZ, Rabe J, Sweadner KJ (2003) Global loss of Na, K-ATPase and its nitric oxide-mediated regulation in a transgenic mouse model of amyotrophic lateral sclerosis. *J Neurosci Off J Soc Neurosci* 23:43–51
17. Enjin A, Rabe N, Nakanishi ST, Vallstedt A, Gezelius H, Memic F, Lind M, Hjalt T, Tourtellotte WG, Bruder C, Eichele G, Whelan PJ, Kullander K (2010) Identification of novel spinal cholinergic genetic subtypes disclose Chodl and Pitx2 as markers for fast motor neurons and partition cells. *J Comp Neurol* 518:2284–2304
18. Ezzi SA, Urushitani M, Julien JP (2007) Wild-type superoxide dismutase acquires binding and toxic properties of ALS-linked mutant forms through oxidation. *J Neurochem* 102:170–178. doi:10.1111/j.1471-4159.2007.04531.x
19. Filezac de L'Etang A, Maharjan N, Cordeiro Brana M, Rueggsegger C, Rehmann R, Goswami A, Roos A, Troost D, Schneider BL, Weis J, Saxena S (2015) Marinesco-Sjogren syndrome protein SIL1 regulates motor neuron subtype-selective ER stress in ALS. *Nat Neurosci*. doi:10.1038/nn.3903
20. Fraser CL, Arieff AI (2001) Na-K-ATPase activity decreases with aging in female rat brain synaptosomes. *Am J Physiol Ren Physiol* 281:F674–F678
21. Fritz E, Izaurieta P, Weiss A, Mir FR, Rojas P, Gonzalez D, Rojas F, Brown RH Jr, Madrid R, van Zundert B (2013) Mutant SOD1-expressing astrocytes release toxic factors that trigger motoneuron death by inducing hyperexcitability. *J Neurophysiol* 109:2803–2814. doi:10.1152/jn.00500.2012
22. Gaudette M, Hirano M, Siddique T (2000) Current status of SOD1 mutations in familial amyotrophic lateral sclerosis. *Amyotroph Lateral Scler Other Motor Neuron Disord* 1:83–89
23. Genet S, Kado RT (1997) Hyperpolarizing current of the Na/K ATPase contributes to the membrane polarization of the Purkinje cell in rat cerebellum. *Pflugers Arch* 434:559–567
24. Gros-Louis F, Soucy G, Lariviere R, Julien JP (2010) Intracerebroventricular infusion of monoclonal antibody or its derived Fab fragment against misfolded forms of SOD1 mutant delays mortality in a mouse model of ALS. *J Neurochem* 113:1188–1199
25. Guareschi S, Cova E, Cereda C, Ceroni M, Donetti E, Bosco DA, Trotti D, Pasinelli P (2012) An over-oxidized form of superoxide dismutase found in sporadic amyotrophic lateral sclerosis with bulbar onset shares a toxic mechanism with mutant SOD1. *Proc Natl Acad Sci USA* 109:5074–5079. doi:10.1073/pnas.1115402109
26. Gunasekera K, Wuthrich D, Braga-Lagache S, Heller M, Ochsenreiter T (2012) Proteome remodelling during development from blood to insect-form *Trypanosoma brucei* quantified by SILAC and mass spectrometry. *BMC Genom* 13:556
27. Gurney ME (1994) Transgenic-mouse model of amyotrophic lateral sclerosis. *N Engl J Med* 331:1721–1722
28. Gurney ME, Pu H, Chiu AY, Dal Canto MC, Polchow CY, Alexander DD, Caliendo J, Hentati A, Kwon YW, Deng HX et al (1994) Motor neuron degeneration in mice that express a human Cu, Zn superoxide dismutase mutation. *Science* 264:1772–1775
29. Hegedus J, Putman CT, Tyreman N, Gordon T (2008) Preferential motor unit loss in the SOD1 G93A transgenic mouse model of amyotrophic lateral sclerosis. *J Physiol* 586:3337–3351
30. Hieber V, Siegel GJ, Fink DJ, Beaty MW, Mata M (1991) Differential distribution of (Na, K)-ATPase alpha isoforms in the central nervous system. *Cell Mol Neurobiol* 11:253–262
31. Ilieva EV, Ayala V, Jove M, Dalfo E, Cacabelos D, Povedano M, Bellmunt MJ, Ferrer I, Pamplona R, Portero-Otin M (2007) Oxidative and endoplasmic reticulum stress interplay in sporadic amyotrophic lateral sclerosis. *Brain* 130:3111–3123
32. Inquimbart P, Moll M, Kohno T, Scholz J (2013) Stereotaxic injection of a viral vector for conditional gene manipulation in the mouse spinal cord. *J Vis Exp* 73:e50313. doi:10.3791/50313
33. Kreutz F, Scherer EB, Ferreira AG, Petry Fdos S, Pereira CL, Santana F, de Souza Wyse AT, Salbego CG, Trindade VM (2013) Alterations on Na(+), K(+)-ATPase and acetylcholinesterase activities induced by amyloid-beta peptide in rat brain and GM1 ganglioside neuroprotective action. *Neurochem Res* 38:2342–2350. doi:10.1007/s11064-013-1145-6



34. Le Masson G, Przedborski S, Abbott LF (2014) A computational model of motor neuron degeneration. *Neuron* 83:975–988. doi:[10.1016/j.neuron.2014.07.001](https://doi.org/10.1016/j.neuron.2014.07.001)
35. Leroy F, Lamotte d'Incamps B, Imhoff-Manuel RD, Zytnicki D (2014) Early intrinsic hyperexcitability does not contribute to motoneuron degeneration in amyotrophic lateral sclerosis. *ELife* 3. doi:[10.7554/eLife.04046](https://doi.org/10.7554/eLife.04046)
36. Liguri G, Taddei N, Nassi P, Latorraca S, Nediani C, Sorbi S (1990) Changes in Na<sup>+</sup>, K<sup>(+)</sup>-ATPase, Ca<sup>2+</sup>-ATPase and some soluble enzymes related to energy metabolism in brains of patients with Alzheimer's disease. *Neurosci Lett* 112:338–342
37. Lingrel JB (2010) The physiological significance of the cardiotonic steroid/ouabain-binding site of the Na, K-ATPase. *Annu Rev Physiol* 72:395–412
38. Liu HN, Tjostheim S, Dasilva K, Taylor D, Zhao B, Rakhit R, Brown M, Chakrabarty A, McLaurin J, Robertson J (2012) Targeting of monomer/misfolded SOD1 as a therapeutic strategy for amyotrophic lateral sclerosis. *J Neurosci Off J Soc Neurosci* 32:8791–8799
39. Liu J, Lillo C, Jonsson PA, Vande Velde C, Ward CM, Miller TM, Subramaniam JR, Rothstein JD, Marklund S, Andersen PM, Brannstrom T, Gredal O, Wong PC, Williams DS, Cleveland DW (2004) Toxicity of familial ALS-linked SOD1 mutants from selective recruitment to spinal mitochondria. *Neuron* 43:5–17
40. Logroscino G, Traynor BJ, Hardiman O, Chio A, Mitchell D, Swigler RJ, Millul A, Benn E, Beghi E (2010) Incidence of amyotrophic lateral sclerosis in Europe. *J Neurol Neurosurg Psychiatry* 81:385–390
41. Mark RJ, Hensley K, Butterfield DA, Mattson MP (1995) Amyloid beta-peptide impairs ion-motive ATPase activities: evidence for a role in loss of neuronal Ca<sup>2+</sup> homeostasis and cell death. *J Neurosci Off J Soc Neurosci* 15:6239–6249
42. McGrail KM, Phillips JM, Sweadner KJ (1991) Immunofluorescent localization of three Na, K-ATPase isozymes in the rat central nervous system: both neurons and glia can express more than one Na, K-ATPase. *J Neurosci Off J Soc Neurosci* 11:381–391
43. Millul A, Beghi E, Logroscino G, Micheli A, Vitelli E, Zardi A (2005) Survival of patients with amyotrophic lateral sclerosis in a population-based registry. *Neuroepidemiology* 25:114–119
44. Munzer JS, Daly SE, Jewell-Motz EA, Lingrel JB, Blostein R (1994) Tissue- and isoform-specific kinetic behavior of the Na, K-ATPase. *J Biol Chem* 269:16668–16676
45. Nishitoh H, Kadowaki H, Nagai A, Maruyama T, Yokota T, Fukutomi H, Noguchi T, Matsuzawa A, Takeda K, Ichijo H (2008) ALS-linked mutant SOD1 induces ER stress- and ASK1-dependent motor neuron death by targeting Derlin-1. *Genes Dev* 22:1451–1464
46. Pambo-Pambo A, Durand J, Gueritaud JP (2009) Early excitability changes in lumbar motoneurons of transgenic SOD1G85R and SOD1G(93A-Low) mice. *J Neurophysiol* 102:3627–3642
47. Piotrkiewicz M, Hausmanowa-Petrusewicz I (2011) Motoneuron afterhyperpolarisation duration in amyotrophic lateral sclerosis. *J Physiol* 589:2745–2754
48. Pisani A, Martella G, Tschertner A, Costa C, Mercuri NB, Bernardi G, Shen J, Calabresi P (2006) Enhanced sensitivity of DJ-1-deficient dopaminergic neurons to energy metabolism impairment: role of Na<sup>+</sup>/K<sup>+</sup> ATPase. *Neurobiol Dis* 23:54–60
49. Pullen AH, Athanasiou D (2009) Increase in presynaptic territory of C-terminals on lumbar motoneurons of G93A SOD1 mice during disease progression. *Eur J Neurosci* 29:551–561
50. Pun S, Santos AF, Saxena S, Xu L, Caroni P (2006) Selective vulnerability and pruning of phasic motoneuron axons in motoneuron disease alleviated by CNTF. *Nat Neurosci* 9:408–419
51. Puttapparthi K, Wojcik C, Rajendran B, DeMartino GN, Elliott JL (2003) Aggregate formation in the spinal cord of mutant SOD1 transgenic mice is reversible and mediated by proteasomes. *J Neurochem* 87:851–860
52. Rakhit R, Crow JP, Lepock JR, Kondejewski LH, Cashman NR, Chakrabarty A (2004) Monomeric Cu, Zn-superoxide dismutase is a common misfolding intermediate in the oxidation models of sporadic and familial amyotrophic lateral sclerosis. *J Biol Chem* 279:15499–15504
53. Rakhit R, Robertson J, Vande Velde C, Horne P, Ruth DM, Griffin J, Cleveland DW, Cashman NR, Chakrabarty A (2007) An immunological epitope selective for pathological monomer-misfolded SOD1 in ALS. *Nat Med* 13:754–759
54. Raoul C, Abbas-Terki T, Bensadoun JC, Guillot S, Haase G, Szulc J, Henderson CE, Aebischer P (2005) Lentiviral-mediated silencing of SOD1 through RNA interference retards disease onset and progression in a mouse model of ALS. *Nat Med* 11:423–428
55. Rotunno MS, Bosco DA (2013) An emerging role for misfolded wild-type SOD1 in sporadic ALS pathogenesis. *Front Cell Neurosci* 7:253. doi:[10.3389/fncel.2013.00253](https://doi.org/10.3389/fncel.2013.00253)
56. Saxena S, Cabuy E, Caroni P (2009) A role for motoneuron subtype-selective ER stress in disease manifestations of FALS mice. *Nat Neurosci* 12:627–636
57. Saxena S, Caroni P (2011) Selective neuronal vulnerability in neurodegenerative diseases: from stressor thresholds to degeneration. *Neuron* 71:35–48
58. Saxena S, Roselli F, Singh K, Leptien K, Julien JP, Gros-Louis F, Caroni P (2013) Neuroprotection through excitability and mTOR required in ALS motoneurons to delay disease and extend survival. *Neuron* 80:80–96
59. Schutz B (2005) Imbalanced excitatory to inhibitory synaptic input precedes motor neuron degeneration in an animal model of amyotrophic lateral sclerosis. *Neurobiol Dis* 20:131–140. doi:[10.1016/j.nbd.2005.02.006](https://doi.org/10.1016/j.nbd.2005.02.006)
60. Shinoda T, Ogawa H, Cornelius F, Toyoshima C (2009) Crystal structure of the sodium-potassium pump at 2.4 Å resolution. *Nature* 459:446–450
61. Tortarolo M, Grignaschi G, Calvaresi N, Zennaro E, Spaltro G, Colovic M, Fracasso C, Guiso G, Elger B, Schneider H, Seilheimer B, Caccia S, Bendotti C (2006) Glutamate AMPA receptors change in motor neurons of SOD1G93A transgenic mice and their inhibition by a noncompetitive antagonist ameliorates the progression of amyotrophic lateral sclerosis-like disease. *J Neurosci Res* 83:134–146. doi:[10.1002/jnr.20715](https://doi.org/10.1002/jnr.20715)
62. Urayama O, Sweadner KJ (1988) Ouabain sensitivity of the alpha 3 isozyme of rat Na, K-ATPase. *Biochem Biophys Res Commun* 156:796–800
63. Urushitani M, Ezzi SA, Julien JP (2007) Therapeutic effects of immunization with mutant superoxide dismutase in mice models of amyotrophic lateral sclerosis. *Proc Natl Acad Sci USA* 104:2495–2500
64. Urushitani M, Ezzi SA, Matsuo A, Tooyama I, Julien JP (2008) The endoplasmic reticulum-Golgi pathway is a target for translocation and aggregation of mutant superoxide dismutase linked to ALS. *FASEB J Off Publ Fed Am Soc Exp Biol* 22:2476–2487
65. Venugopal S, Hsiao CF, Sonoda T, Wiedau-Pazos M, Chandler SH (2015) Homeostatic dysregulation in membrane properties of masticatory motoneurons compared with oculomotor neurons in a mouse model for amyotrophic lateral sclerosis. *J Neurosci Off J Soc Neurosci* 35:707–720. doi:[10.1523/JNEUROSCI.1682-14.2015](https://doi.org/10.1523/JNEUROSCI.1682-14.2015)
66. Vucic S, Kiernan MC (2010) Upregulation of persistent sodium conductances in familial ALS. *J Neurol Neurosurg Psychiatry* 81:222–227
67. Vucic S, Nicholson GA, Kiernan MC (2008) Cortical hyperexcitability may precede the onset of familial amyotrophic lateral sclerosis. *Brain* 131:1540–1550

68. Wainger BJ, Kiskinis E, Mellin C, Wiskow O, Han SS, Sandoe J, Perez NP, Williams LA, Lee S, Boulting G, Berry JD, Brown RH Jr, Cudkowicz ME, Bean BP, Eggen K, Woolf CJ (2014) Intrinsic membrane hyperexcitability of amyotrophic lateral sclerosis patient-derived motor neurons. *Cell Rep* 7:1–11. doi:[10.1016/j.celrep.2014.03.019](https://doi.org/10.1016/j.celrep.2014.03.019)
69. Wroe R, Wai-Ling Butler A, Andersen PM, Powell JF, Al-Chalabi A (2008) ALSOD: the amyotrophic lateral sclerosis online database. *Amyotroph Lateral Scler* 9:249–250
70. Zhang D, Hou Q, Wang M, Lin A, Jarzylo L, Navis A, Raissi A, Liu F, Man HY (2009) Na, K-ATPase activity regulates AMPA receptor turnover through proteasome-mediated proteolysis. *J Neurosci Off J Soc Neurosci* 29:4498–4511. doi:[10.1523/JNEUROSCI.6094-08.2009](https://doi.org/10.1523/JNEUROSCI.6094-08.2009)